Calibrating spectrometers for measurements of the spectral irradiance caused by solar radiation

OPEN ACCESS
IOP Publishing
Metrologia
Metrologia **57** (2020) 065027 (27pp)
https://doi.org/10.1088/1681-7575/abafc5

Calibrating spectrometers for measurements of the spectral irradiance caused by solar radiation

Carsten Schinke[1,2], Hendrik Pollex[1], David Hinken[1], Martin Wolf[1], Karsten Bothe[1], Ingo Kröger[3], Saulius Nevas[3] and Stefan Winter[3]

[1] Institute for Solar Energy Research Hamelin (ISFH), Am Ohrberg 1, 31860 Emmerthal, Germany
[2] Leibniz University of Hanover (LUH), Institute for Solid State Physics, Appelstraße 2, 30167 Hannover, Germany
[3] Physikalisch-Technische Bundesanstalt (PTB), Bundesalle 100, 38116 Braunschweig, Germany

E-mail: schinke@isfh.de

Received 18 June 2020, revised 30 July 2020
Accepted for publication 17 August 2020
Published 28 October 2020

Abstract

Measuring the spectral irradiance of solar radiation is required in many fields of science and technology. In this work, we present an in-depth discussion of the measuring procedure and required corrections for such measurements. We also describe our measurement uncertainty analysis, which is based on a Monte-Carlo procedure in accordance with the *Guide to the expression of uncertainty in measurement* (JCGM, Paris, 2008). For this purpose, fifteen uncertainty sources are identified, analyzed and described analytically. As a specific application example, we describe the instrumentation and procedure for determining the spectral irradiance of a solar simulator at the ISO/IEC 17 025 accredited solar cell calibration laboratory ISFH CalTeC and the corresponding measurement uncertainty analysis. Moreover, we provide a Python implementation for this calculation along with the paper. We show that for state-of-the-art instrumentation, significant uncertainty contributions arise from the reference lamp (primary calibration standard), stray light and signal-to-noise ratio. If sharp spectral features are present (which is common, e.g. for Xenon lamps), spectral bandwidth and wavelength uncertainty also contribute significantly to the overall uncertainty.

Keywords: spectral irradiance, solar radiation, measurement uncertainty analysis, spectrometer, spectroradiometer, calibration, solar simulator

(Some figures may appear in colour only in the online journal)

1. Introduction

Measuring the spectral irradiance of solar radiation is required in many fields of science and technology such as meteorology or solar energy. Accordingly, many laboratories routinely operate spectrometers for the acquisition of spectral irradiance data, and a variety of different instruments are in use. Array spectrometers are frequently chosen for this purpose due to their compactness and their ability to acquire the spectral irradiance over a wide wavelength range within just a few seconds. However, the measured spectral irradiance distribution is influenced by several effects that eventually require a correction, e.g. distance adjustment of the measuring head, changes of the detector temperature, non-linearities or stray light. These effects are often pronounced when using array spectrometers compared to grating monochromator systems. Recent intercomparisons of solar spectral irradiance measurements

between different laboratories show deviations of the order of 10% [1–3], emphasizing the significance of deviations occurring during such measurements and the need for a thorough analysis of the measured data in order to facilitate a correct interpretation.

The interpretation of measurement results is supported by substantiated estimates of the corresponding measurement uncertainty. Results of uncertainty analyses for spectral irradiance measurements have been presented in the literature [4–16]. However, these publications either focus on the characterization of specific instruments or only give a brief explanation of the underlying methodology. In this work, we therefore focus on the methodology rather than specific instrumentation in order to provide a guide to the implementation of the measurement and uncertainty analysis procedure. Since spectral irradiance data are often further processed in spectral integrals (e.g. for the calculation of the spectral mismatch correction factor used in solar cell calibration), correlations of the data with respect to wavelength need to be taken into account by the uncertainty analysis. This is ensured by the procedure laid out in this work, which is based on a Monte-Carlo approach according to the *Guide to the Expression of Uncertainty in Measurement* (GUM) [17] (supplement 1). Although the paper mainly addresses indoor measurements in the laboratory (solar simulator) using array spectrometers, which is a typical application case, the methodology can be generalized to outdoor measurements of solar radiation and scanning grating monochromator systems as long as similar measurement geometries prevail, e.g. if direct radiation is considered.

In the first part of the paper, we discuss the measuring procedure and present an in-depth discussion of required corrections to the measured data and the quantification of measurement uncertainty contributions. In the second part of the paper, we describe the procedure and uncertainty analysis for the measurement of the spectral irradiance of the solar simulator at the ISO/IEC 17 025 accredited solar cell calibration laboratory ISFH CalTeC as a specific application example. We ensure the traceability of the measurement results to national standards by calibrating the spectrometer and present a sensitivity analysis for the various uncertainty contributions in order to identify the dominant sources of uncertainty. Python code containing the uncertainty calculation for our application example will be made available under an open source license by the time of publication on the website of ISFH CalTeC, allowing everyone to reproduce the results presented in this work and to adapt the procedure to own requirements.

2. Measuring procedure

The spectral irradiance $E_\lambda^{\mathrm{DUT}}(\lambda)$ of the *device under test* (DUT, which is a solar simulator or the Sun in this paper) at wavelength λ is determined with a calibrated spectrometer. In general, the spectrometer calibration is carried out using a reference lamp with known spectral irradiance $E_\lambda^{\mathrm{Ref}}(\lambda)$. For practical reasons, the spectrometer calibration normally determines the *radiometric correction function* $K(\lambda)$ for the spectrometer, which is stored as a data set and applied to the DUT measurements carried out later on, instead of performing a direct substitution measurement. It is common for many laboratories to determine $K(\lambda)$ themselves. Thus, we describe the procedure for (a) the reference measurement for the determination of the radiometric correction function and (b) the spectral irradiance of the DUT. Both measurements have to be corrected for various effects in order to determine $E_\lambda^{\mathrm{DUT}}(\lambda)$ correctly, as outlined in the following.

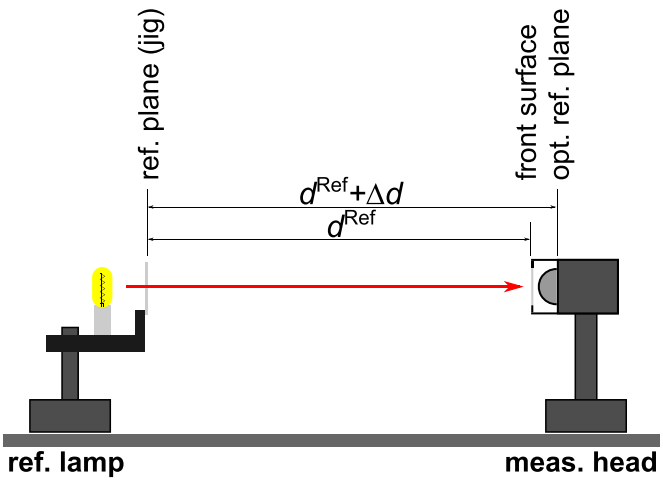

Figure 1. Sketch of the measuring geometry.

2.1. Reference measurement / Radiometric correction function

The determination of the radiometric correction function $K(\lambda)$ requires the acquisition of the detector signal $S_1^{\mathrm{Ref}}(\lambda)$ when the measuring head of the spectrometer is irradiated by the reference lamp. For this purpose, the distance between the reference lamp and the measuring head needs to be adjusted to the distance d^{Ref} for which $E_\lambda^{\mathrm{Ref}}(\lambda)$ is specified in the lamp's calibration certificate. For the reference lamp, the reference plane for the distance measurement is usually defined by an adjustment aid (jig) or the lamp holder. This information is contained in its calibration certificate. The optical reference plane of the measuring head does not necessarily coincide with its front surface, which is often used for the distance measurement, but may lie inside the measuring head as sketched in figure 1. There are two options for taking the offset Δd between front surface and optical reference plane into account during the determination of $S_1^{\mathrm{Ref}}(\lambda)$: First, the distance between reference plane of the lamp and the front surface of the measuring head can be adjusted to the effective distance

$$d_{\mathrm{eff}} = d^{\mathrm{Ref}} - \Delta d\,, \tag{1}$$

so that the actual distance between the optical reference planes is d^{Ref}. Second, if a distance adjustment is not possible, a mathematical correction of $S_1^{\mathrm{Ref}}(\lambda)$ can be performed by applying a multiplicative correction factor c_{dist} later in equation (10). An option for the experimental determination of Δd is described in appendix B.

In order to take measurement noise into account, $S_1^{\mathrm{Ref}}(\lambda)$ is usually acquired N times and the average signal is used. As discussed in section 3, $N \geq 25$ should be chosen. This yields

$$S_1^{\mathrm{Ref}}(\lambda) = \frac{1}{N}\sum_{i=1}^{N} S_{1,i}^{\mathrm{Ref}}(\lambda)\ . \tag{2}$$

Next, the spectrometer signal must be corrected for detector dark signal and external stray light from the surrounding by subtracting these signal contributions. Some spectrometers also require a correction of the measured signal with respect to detector temperature. The dark signal $S_{\mathrm{dark}}^{\mathrm{Ref}}(\lambda)$ can be acquired by placing a cap on the measuring head of the spectrometer. Many instruments also feature an internal shutter for this purpose. A common approach for determining the external stray light signal $S_{\mathrm{stray,ext}}^{\mathrm{Ref}}(\lambda)$ is placing a beam block in the beam path, which blocks only the light coming directly from the reference lamp. Both measurements are carried out using the same integration time as for $S_1^{\mathrm{Ref}}(\lambda)$. As for $S_1^{\mathrm{Ref}}(\lambda)$, the measurements are repeated N times in order to take measurement noise into account. It is usually advantageous to acquire a *combined background signal*

$$S_{\mathrm{bgnd}}^{\mathrm{Ref}}(\lambda) = S_{\mathrm{dark}}^{\mathrm{Ref}}(\lambda) + S_{\mathrm{stray,ext}}^{\mathrm{Ref}}(\lambda) \tag{3}$$

if such a measurement is facilitated by the spectrometer. For the purpose of temperature correction, a multiplicative correction factor $c_{\mathrm{temp}}(T_1^{\mathrm{Ref}}, \lambda)$ can be applied to the background-corrected signal, which depends on the wavelength λ and the detector temperature T_1^{Ref} during the measurements in general. If $S_1^{\mathrm{Ref}}(\lambda)$ and $S_{\mathrm{stray,ext}}^{\mathrm{Ref}}(\lambda)$ have units of digital counts, the signal is subsequently normalized to integration time ($t_{\mathrm{int}}^{\mathrm{Ref}}$) in order to enable the use of a different integration time later on for the DUT measurement described in the next section. Expressed mathematically, the corrected signal is

$$S_2^{\mathrm{Ref}}(\lambda) = \frac{S_1^{\mathrm{Ref}}(\lambda) - S_{\mathrm{bgnd}}^{\mathrm{Ref}}(\lambda)}{t_{\mathrm{int}}^{\mathrm{Ref}}} \cdot c_{\mathrm{temp}}(\lambda, T_1^{\mathrm{Ref}})\ . \tag{4}$$

The temperature correction procedure assumes that the detector temperature is constant during the measurements of $S_1^{\mathrm{Ref}}(\lambda)$ and $S_{\mathrm{bgnd}}^{\mathrm{Ref}}(\lambda)$, which is usually justified when using array spectrometers with integration times of the order of milliseconds or seconds and performing the measurements in direct succession. The temperature correction factor needs to be determined for each individual instrument. One option for the experimental determination of this factor is measuring the signal change under artificial heating of the instrument while the measuring head is irradiated by a stable light source. This procedure is described in more detail in appendix C. For spectrometers with temperature-controlled detectors, the correction is often negligible, i.e. $c_{\mathrm{temp}} \equiv 1$ can be assumed. If the spectrometer outputs the signals in units of digital counts per time, i.e. the normalization is already performed by the instrument, the division by $t_{\mathrm{int}}^{\mathrm{Ref}}$ is omitted in the latter equation. There are instruments which determine the detector dark signal automatically for each measurement using an internal shutter and thus do not facilitate a combined background signal measurement. For such instruments, a separate measurement of the external stray light signal $S_{\mathrm{stray,ext}}^{\mathrm{Ref}}(\lambda)$ must be performed, which requires an additional dark signal measurement $S_{\mathrm{dark}}^{\mathrm{stray}}(\lambda)$ and thereby introduces additional measurement noise.

Having obtained the background and temperature corrected signal $S_2^{\mathrm{Ref}}(\lambda)$, non-linearity corrections with regard to irradiance level and integration time t_{int} may be required for some spectrometers. These corrections can again be expressed by multiplicative correction factors $c_{\mathrm{lin,irr}}\left(S_2^{\mathrm{Ref}}(\lambda)\right)$ and $c_{\mathrm{lin,tint}}(t_{\mathrm{int}}^{\mathrm{Ref}}, \lambda)$, which depend on the measured signal and the integration time and need to be determined experimentally for each individual instrument (see appendix D). Application of the correction factors yields

$$S_3^{\mathrm{Ref}}(\lambda) = S_2^{\mathrm{Ref}}(\lambda) \cdot c_{\mathrm{lin,irr}}\left(S_2^{\mathrm{Ref}}(\lambda)\right) c_{\mathrm{lin,tint}}(t_{\mathrm{int}}^{\mathrm{Ref}}, \lambda)\ . \tag{5}$$

For state-of-the-art spectrometers, both corrections are often negligible, i.e. $c_{\mathrm{lin,irr}} \equiv 1$ and $c_{\mathrm{lin,tint}} \equiv 1$.

Next, the spectrometer signal $S_3^{\mathrm{Ref}}(\lambda)$ needs to be corrected for internal (also called spectral) stray light and subsequently for spectral bandwidth. A widely applied method for the correction of internal stray light was developed by Zong *et al* [18]. It consists of a multiplication of the signal vector $\boldsymbol{S}_3^{\mathrm{Ref}}$ (which is the signal $S_3^{\mathrm{Ref}}(\lambda)$ written as a vector, i.e. element i of the vector represents $S_3^{\mathrm{Ref}}(\lambda_i)$), with a spectral stray light correction matrix $\mathbf{C}_{\mathrm{corr}}$:

$$\boldsymbol{S}_4^{\mathrm{Ref}} = \mathbf{C}_{\mathrm{corr}}\boldsymbol{S}_3^{\mathrm{Ref}}\ . \tag{6}$$

The stray light correction matrix $\mathbf{C}_{\mathrm{corr}}$ is determined from measurements with monochromatic irradiation of the measuring head, from which the stray light response of the spectrometer can be assessed. After stray light correction, the signal vector $\boldsymbol{S}_4^{\mathrm{Ref}}$ is converted back into a signal function $S_4^{\mathrm{Ref}}(\lambda)$.

For the correction of spectral bandwidth effects, several methods have been proposed in the literature [19–22]. These corrections can be expressed mathematically as a multiplication of the spectrometer signal $S_4^{\mathrm{Ref}}(\lambda)$ with a correction factor $c_{\mathrm{bw}}(\Delta\lambda, \lambda)$, which depends on the spectral bandwidth $\Delta\lambda$, giving

$$S_5^{\mathrm{Ref}}(\lambda) = S_4^{\mathrm{Ref}}(\lambda) \cdot c_{\mathrm{bw}}\left(S_4^{\mathrm{Ref}}(\lambda), \Delta\lambda\right)\ . \tag{7}$$

In this paper, we define the spectral bandwidth $\Delta\lambda$ as the wavelength interval $[\lambda - \Delta\lambda/2, \lambda + \Delta\lambda/2]$ around the nominal wavelength λ, within which the transmittance of the monochromator (slit function) is greater then zero. We use the analytical formula [21]

$$c_{\mathrm{bw}}(S, \Delta\lambda) = 1 - \frac{S(\lambda - \Delta\lambda/2) + S(\lambda + \Delta\lambda/2) - 2S(\lambda)}{12\,S(\lambda)} \tag{8}$$

for spectral bandwidth correction, where $S(\lambda)$ is the detector signal. Equation (8) assumes a triangular bandpass function, which holds for an ideal monochromator (see discussion in

section 3.3.7). The derivation of this formula is outlined in appendix E.

Having performed all corrections as described above, the distance correction factor c_{dist} is finally applied to $S_5^{\mathrm{Ref}}(\lambda)$. Under the assumption that the reference lamp can be regarded as a point light source, i.e. the lateral extension of the reference lamp is small compared to d^{Ref},

$$c_{\mathrm{dist}} = \left(\frac{d+\Delta d}{d^{\mathrm{Ref}}}\right)^2 \tag{9}$$

follows from the inverse square law for point light sources, where d is the actual measuring distance.. If d is adjusted to d_{eff} for the measurement as described above, $c_{\mathrm{dist}} \equiv 1$ holds. With the distance correction, the radiometric correction function of the spectrometer finally follows as

$$K(\lambda) = \frac{E_\lambda^{\mathrm{Ref}}(\lambda)}{S_5^{\mathrm{Ref}}(\lambda)} \cdot c_{\mathrm{dist}} \,. \tag{10}$$

Note that the distance correction may be omitted, i.e. $c_{\mathrm{dist}} \equiv 1$, if only a relative spectral irradiance of the DUT is required (e.g. in spectral mismatch calculations for solar cell calibrations according to the IEC 60 904-7 standard [23]).

2.2. Spectral irradiance of DUT

In order to obtain the spectral irradiance $E_\lambda^{\mathrm{DUT}}(\lambda)$ of the DUT, the measuring head of the spectrometer is now placed in the light field and the signal $S_1^{\mathrm{DUT}}(\lambda)$ is acquired. As for the reference measurement, $S_{1,i}^{\mathrm{DUT}}(\lambda)$ is acquired N times, temperature corrections are eventually applied and the mean value $S_1^{\mathrm{DUT}}(\lambda)$ is used for further calculations. A similar sequence of corrections as for $S_1^{\mathrm{Ref}}(\lambda)$ has to be applied to $S_1^{\mathrm{DUT}}(\lambda)$. However, external stray light is not corrected here because the intention of the measurement is to acquire the spectral irradiance in the measuring plane 'as is'. Therefore, only the detector dark signal $S_{\mathrm{dark}}^{\mathrm{DUT}}(\lambda)$ is subtracted. Note that additional corrections for the angular sensitivity of the measuring head may be required if radiation incident from a solid angle much larger than during the reference measurement is considered, which is the case, for instance, when measuring global spectral irradiance of natural sunlight [24–26]. This is, however, beyond the scope of this paper. Also, note that as for the reference measurement, the measuring plane is defined by the optical reference plane of the measuring head. In analogy to equations (4) through (8), we obtain

$$\begin{aligned}
S_2^{\mathrm{DUT}}(\lambda) &= \frac{S_1^{\mathrm{DUT}}(\lambda) - S_{\mathrm{dark}}^{\mathrm{DUT}}(\lambda)}{t_{\mathrm{int}}^{\mathrm{DUT}}} \cdot c_{\mathrm{temp}}(\lambda, T_1^{\mathrm{DUT}}) \,, \\
S_3^{\mathrm{DUT}}(\lambda) &= S_2^{\mathrm{DUT}}(\lambda) \cdot c_{\mathrm{lin,irr}}\left(S_2^{\mathrm{DUT}}(\lambda)\right) c_{\mathrm{lin,tint}}(t_{\mathrm{int}}^{\mathrm{DUT}}) \,, \\
\boldsymbol{S}_4^{\mathrm{DUT}} &= \mathbf{C}_{\mathrm{corr}}\, \boldsymbol{S}_3^{\mathrm{DUT}} \,, \\
S_5^{\mathrm{DUT}}(\lambda) &= S_4^{\mathrm{DUT}}(\lambda)\, c_{\mathrm{bw}}\left(S_4^{\mathrm{DUT}}(\lambda), \Delta\lambda, \lambda\right) \,.
\end{aligned} \tag{11}$$

The spectral irradiance $E_\lambda^{\mathrm{DUT}}(\lambda)$ then finally follows as

$$E_\lambda^{\mathrm{DUT}}(\lambda) = S_5^{\mathrm{DUT}}(\lambda)\, K(\lambda) = \frac{S_5^{\mathrm{DUT}}(\lambda)}{S_5^{\mathrm{Ref}}(\lambda)}\, c_{\mathrm{dist}}\, E_\lambda^{\mathrm{Ref}}(\lambda) \,. \tag{12}$$

3. Measurement uncertainty analysis

3.1. Methodology

Determining the measurement uncertainty is an integral part of a calibration. The measurement uncertainty analysis presented in the following is based on the methodology specified in the GUM [17]. We conduct an uncertainty analysis based on a Monte-Carlo approach as described in the GUM supplement 1. The basic idea of this approach is the recalculation of the measurement result $E_\lambda^{\mathrm{DUT}}(\lambda)$ many times, while all input quantities are altered on each iteration according to their uncertainties, the uncertainty distribution functions and the underlying model of impact on $E_\lambda^{\mathrm{DUT}}(\lambda)$. The resulting distribution of $E_\lambda^{\mathrm{DUT}}(\lambda)$ then directly yields an estimate of its uncertainty.

Figure 2 shows an Ishikawa diagram of all identified sources of uncertainty for the determination of $E_\lambda^{\mathrm{DUT}}(\lambda)$. Each of these components affects the result of the measurement in a specific way, which can mathematically be expressed by a multiplicative f-factor, namely:

- Measurement noise $f_{\mathrm{noise}}^{X(\lambda)}$,
- internal background (dark signal) $f_{\mathrm{dark}}^{X(\lambda)}$,
- external stray light $f_{\mathrm{stray,ext}}^{\mathrm{Ref}}(\lambda)$,
- internal (spectral) stray light $f_{\mathrm{stray,int}}^{X(\lambda)}$,
- non-linearity of the detector with respect to irradiance levels and integration times $f_{\mathrm{lin,irr}}^{X(\lambda)}, f_{\mathrm{lin,tint}}^{X(\lambda)}$,
- spectral bandwidth $f_{\mathrm{bw}}^{X(\lambda)}$,
- wavelength accuracy $f_{\mathrm{wl}}^{X(\lambda)}$,
- tilt of the measuring head with respect to the optical axis f_{tilt}^{X},
- uncertainty of the known spectral irradiance of the reference lamp $f_{\mathrm{Eref}}(\lambda)$ (usually stated in its calibration certificate),
- distance adjustment during the reference measurement f_{dist},
- stability and adjustment uncertainty of reference lamp operating current $f_{\mathrm{cur}}(\lambda)$,
- reproducibility of the radiometric correction $f_{\mathrm{rep}}(\lambda)$,
- temperature effects of the detector $f_{\mathrm{temp}}(\lambda)$,
- lateral non-uniformity of the light field $f_{\mathrm{non-u}}^{\mathrm{DUT}}(\lambda)$ and
- temporal stability of the DUT $f_{\mathrm{stab-t}}^{\mathrm{DUT}}(\lambda)$.

Some of the factors are different for the reference and DUT measurement, indicated by a superscript. Factors marked with X refer to both measurements ($X = \{\mathrm{Ref}, \mathrm{DUT}\}$). Most of the factors are wavelength dependent, indicated by (λ). The individual f-factors can be combined into a factor $f_{\mathrm{MC}}(\lambda)$, which is recalculated on each Monte-Carlo iteration i. The determination of the f-factors is discussed in detail in the following section 3.3. According to the Ishikawa diagram in figure 2 and equation (12),

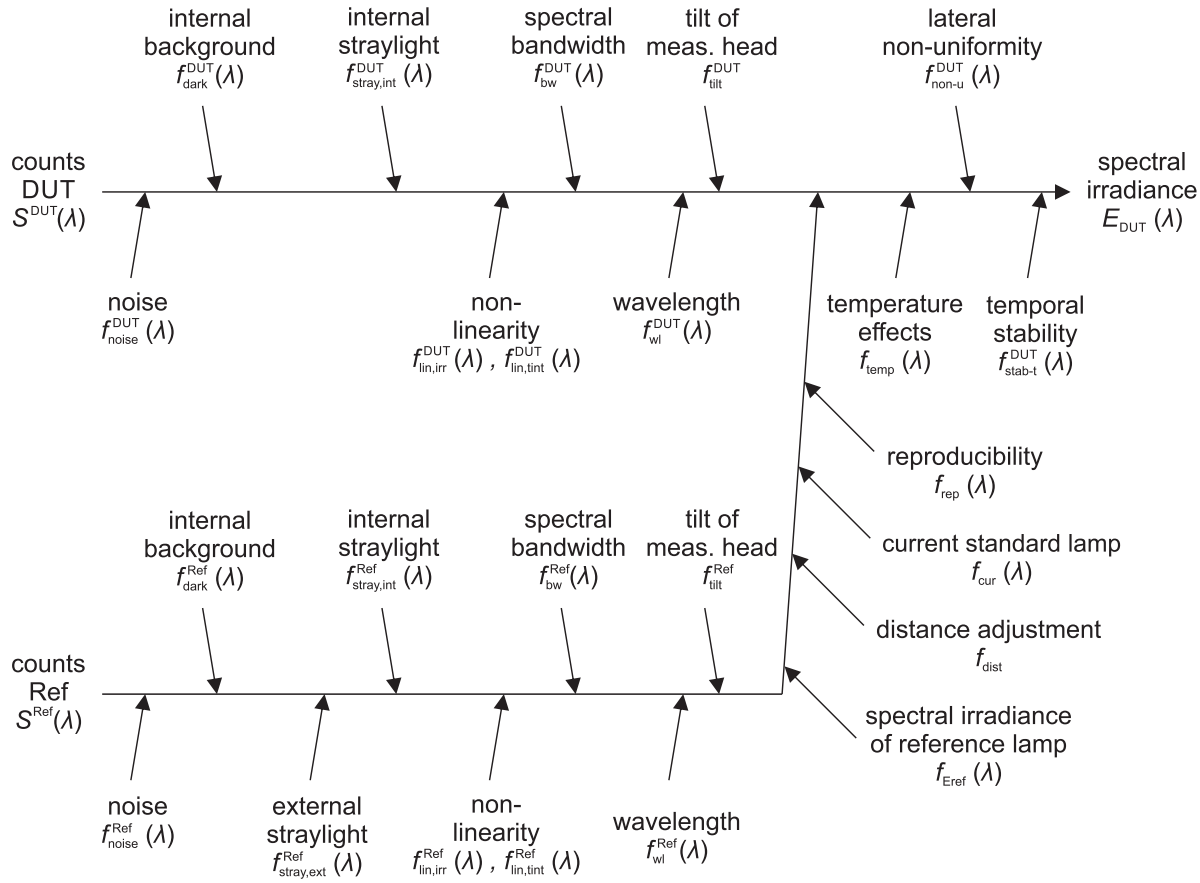

Figure 2. Ishikawa diagram of the measurement uncertainties that contribute to the calibration of the spectral irradiance measurement of the DUT. The lower branch describes the measurement uncertainties of the radiometric correction function $K(\lambda)$.

$$
\begin{aligned}
f_{\mathrm{MC},i}(\lambda) \;=\; & \frac{f^{\mathrm{DUT}}_{\mathrm{noise}}(\lambda) f^{\mathrm{DUT}}_{\mathrm{dark}}(\lambda) f^{\mathrm{DUT}}_{\mathrm{stray,int}}(\lambda) f^{\mathrm{DUT}}_{\mathrm{lin,irr}}(\lambda) f^{\mathrm{DUT}}_{\mathrm{lin,tint}}(\lambda) f^{\mathrm{DUT}}_{\mathrm{bw}}(\lambda) f^{\mathrm{DUT}}_{\mathrm{wl}}(\lambda) f^{\mathrm{DUT}}_{\mathrm{tilt}}}{f^{\mathrm{Ref}}_{\mathrm{noise}}(\lambda) f^{\mathrm{Ref}}_{\mathrm{dark}}(\lambda) f^{\mathrm{Ref}}_{\mathrm{stray,ext}}(\lambda) f^{\mathrm{Ref}}_{\mathrm{stray,int}}(\lambda) f^{\mathrm{Ref}}_{\mathrm{lin,irr}}(\lambda) f^{\mathrm{Ref}}_{\mathrm{lin,tint}}(\lambda) f^{\mathrm{Ref}}_{\mathrm{bw}}(\lambda) f^{\mathrm{Ref}}_{\mathrm{wl}}(\lambda) f^{\mathrm{Ref}}_{\mathrm{tilt}}} \\
\times \;\; & f_{\mathrm{Eref}}(\lambda) f_{\mathrm{dist}} f_{\mathrm{cur}}(\lambda) f_{\mathrm{rep}}(\lambda) f_{\mathrm{temp}}(\lambda) f^{\mathrm{DUT}}_{\mathrm{non-u}}(\lambda) f^{\mathrm{DUT}}_{\mathrm{stab-t}}(\lambda) \; . \qquad (13)
\end{aligned}
$$

We then calculate the spectral irradiance $E^{\mathrm{DUT}}_{\lambda,i}(\lambda)$ in each Monte-Carlo iteration as

$$
E^{\mathrm{DUT}}_{\lambda,i}(\lambda) = E^{\mathrm{DUT}}_{\lambda}(\lambda) \cdot f_{\mathrm{MC},i}(\lambda) \; , \qquad (14)
$$

where $E^{\mathrm{DUT}}_{\lambda}(\lambda)$ is the measured spectral irradiance of the solar simulator according to equation (12) and already contains all corrections mentioned in section 2. Note that the sources of uncertainty listed here refer to state-of-the-art spectrometers as typically used in calibration laboratories. Especially when using low-cost spectrometers, there may be additional uncertainty contributions or additional corrections that need to be included in the evaluation.

3.2. Correlations

For the correct determination of uncertainty, it is important to consider that some uncertainty contributions affect the whole measured spectral distribution in a similar manner, while others have a different effect at each wavelength. Uncertainty contributions that affect the whole spectral distribution in a similar manner introduce correlations with respect to wavelength. This holds for the contributions due to detector linearity, tilt of the measuring head, distance adjustment, operating current of the lamp, temporal stability of the radiometric correction (reproducibility), temperature effects, lateral non-uniformity and temporal stability of the DUT light source. Moreover, wavelength calibration and spectral bandwidth of the spectrometer introduce wavelength dependent correlations between

reference and DUT measurement. Accounting for such correlations is important for further processing in spectral integrals, e.g. for solar simulator spectral mismatch correction according to the IEC 60 904-7 standard [23]. In order to correctly take correlations into account in the Monte-Carlo analysis, the f-factors have to be calculated in the correct order and correct places in the algorithm as shown in the flow chart in figure 3. The Monte-Carlo analysis implements two nested loops, one for the N Monte-Carlo iterations and an inner one for looping over wavelength λ. Depending on whether an uncertainty contribution affects the whole spectral distribution or not, the random number defining the specific value of the corresponding f-factor is obtained before or within the inner loop. In order to account for correlations between reference and DUT measurement, the same random numbers are used for the corresponding f-factors. In total, 20 random numbers are drawn in each Monte-Carlo iteration using a random number generator. Details on the generation of random numbers can be found in the relevant literature, e.g. [27] and [28]. Depending on the type of uncertainty contribution, the random numbers have different probability distributions as discussed in the following section. In the flow chart, this is represented by greek letters ρ, ν and τ. Having determined the specific values of all f-factors in Monte-Carlo iteration i, $E^{\mathrm{DUT}}_{\lambda,i}(\lambda)$ is calculated according to equation (14). Having finished the Monte-Carlo runs, a histogram is calculated from $E^{\mathrm{DUT}}_{\lambda,i}(\lambda)$. Mean value and width of this distribution correspond to the result of the calculation and its combined uncertainty, respectively. In the usual case that a normal distribution results from the Monte-Carlo analysis, the result $E^{\mathrm{DUT}}_{\lambda,\mathrm{MC}}(\lambda)$ and its combined uncertainty $u_{\mathrm{c}}\left(E^{\mathrm{DUT}}_{\lambda,\mathrm{MC}}(\lambda)\right)$ can be calculated by the standard formulas

$$E^{\mathrm{DUT}}_{\lambda,\mathrm{MC}}(\lambda) = \frac{1}{N}\sum_{i=1}^{N} E^{\mathrm{DUT}}_{\lambda,i}(\lambda) \tag{15}$$

and

$$u_{\mathrm{c}}\left(E^{\mathrm{DUT}}_{\lambda,\mathrm{MC}}(\lambda)\right) = \sqrt{\frac{1}{(N-1)}\sum_{i=1}^{N}\left(E^{\mathrm{DUT}}_{\lambda,i}(\lambda) - E^{\mathrm{DUT}}_{\lambda}(\lambda)\right)^2}. \tag{16}$$

From this combined uncertainty, the expanded uncertainty $U = k\,u_{\mathrm{c}}$ is obtained by multiplication with a suitable expansion factor k (often 2). Having finished the Monte-Carlo calculation, it should be tested that $E^{\mathrm{DUT}}_{\lambda,\mathrm{MC}}(\lambda)$ is similar to $E^{\mathrm{DUT}}_{\lambda}(\lambda)$ as directly following from the measurement according to equation (12). Significant deviations between these two quantities may point towards too small a number of Monte-Carlo iterations. Moreover, it should be tested that the distribution of $E^{\mathrm{DUT}}_{\lambda,i}(\lambda)$ is well defined, i.e. the discrete distribution can be approximated by a continuous function, so that meaningful results are deduced from the Monte-Carlo analysis. Some guidance on choosing the number of Monte-Carlo iterations is provided in the GUM supplement 1.

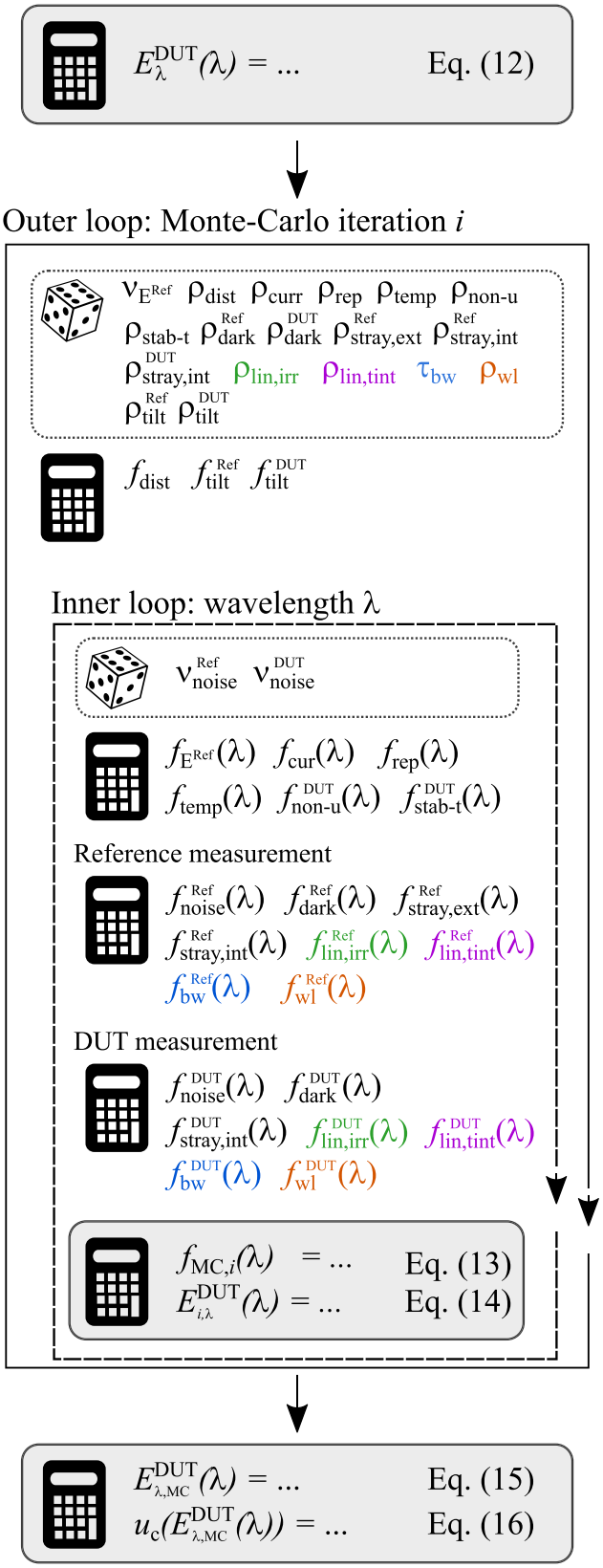

Figure 3. Flow chart for Monte-Carlo analysis. The dice symbolizes the determination of random numbers using a random number generator. Factors depending on the same random numbers are highlighted by coloring. The dice and calculator icons are provided by simpleicon.com and freesvg.org.

3.3. Uncertainty contributions

In a Monte-Carlo analysis, different probability distributions for the input quantities are taken into account by generating random numbers with the corresponding probability distribution. In this work, we use the symbol ν for normally distributed random numbers with mean 0 and standard deviation 1. The symbol ρ represents random numbers which are rectangularly distributed on the interval $(-1, 1)$, whereas τ represents triangularly distributed random numbers on the interval $(-1, 1)$. The following considerations sometimes refer to both $S^{\mathrm{Ref}}(\lambda)$ and $S^{\mathrm{DUT}}(\lambda)$. In this case, $S^X(\lambda)$ is used as a synonym for both quantities. We consider the following uncertainty contributions:

3.3.1. Measurement noise. Spectrometer measurements generally suffer from photon noise, thermal noise of the detector and noise of the measurement amplifier electronics. In order to take this statistical noise into account, N repeated measurement are usually performed. From these measurements, the mean value

$$S^X(\lambda) = \frac{1}{N}\sum_{i=1}^{N} S^X{}_i(\lambda) \tag{17}$$

and the standard uncertainty of the mean value

$$u^X_{\mathrm{noise}}(\lambda) = \sqrt{\frac{1}{N(N-1)}\sum_{i=1}^{N}\left(S^X{}_i(\lambda) - S^X(\lambda)\right)^2} \tag{18}$$

can be determined, where the latter equation represents the standard deviation of the mean value $S^X(\lambda)$. Note that the above equations assume normally distributed quantities, whereas a limited number of measurements is rather described by the Student's t-distribution. However, the t-distribution approaches the normal distribution for a large number of measurements. For 25 repetitions, the deviation between the t-distribution and the normal distribution is already of the order of only 5% rel. A number of 25 repetitions is thus advised to be a good trade-off between measurement time and accuracy. If a drift of the signal occurs during the course of the N measurements, this must be corrected in order to obtain a meaningful standard deviation. One option for this is monitoring the drift by using an additional detector, e.g. a photodiode, and using the ratio of monitor and spectrometer signal. Note that this may introduce additional noise.

Uncertainties due to measurement noise apply independently to all measurements carried out during the measuring procedure, i.e. $S_1^{\mathrm{Ref}}(\lambda)$, $S_{\mathrm{bgnd}}^{\mathrm{Ref}}(\lambda)$, $S_1^{\mathrm{DUT}}(\lambda)$ and $S_{\mathrm{dark}}^{\mathrm{DUT}}(\lambda)$. We thus calculate combined noise uncertainty contributions $u_{\mathrm{noise}}^{\mathrm{Ref}}(\lambda)$ and $u_{\mathrm{noise}}^{\mathrm{DUT}}(\lambda)$ for the corrected signals $S_4^{\mathrm{Ref}}(\lambda)$ and $S_4^{\mathrm{DUT}}(\lambda)$, respectively, which enter the calculation of $E_\lambda^{\mathrm{DUT}}(\lambda)$. According to equations (2) through (11) and the GUM formalism [17],

$$\begin{aligned} u_{\mathrm{noise}}^{\mathrm{Ref}}(\lambda) &= \sqrt{u^2_{S_1^{\mathrm{Ref}}}(\lambda) + u^2_{S_{\mathrm{bgnd}}^{\mathrm{Ref}}}(\lambda)}\,, \\ u_{\mathrm{noise}}^{\mathrm{DUT}}(\lambda) &= \sqrt{u^2_{S_1^{\mathrm{DUT}}}(\lambda) + u^2_{S_{\mathrm{dark}}^{\mathrm{DUT}}}(\lambda)}\,. \end{aligned} \tag{19}$$

With these combined uncertainties, we obtain the f-factors

$$\begin{aligned} f_{\mathrm{noise}}^{\mathrm{Ref}}(\lambda) &= 1 + \frac{u_{\mathrm{noise}}^{\mathrm{Ref}}(\lambda)}{S_2^{\mathrm{Ref}}(\lambda)} \cdot \nu_{\mathrm{noise}}^{\mathrm{Ref}}\,, \\ f_{\mathrm{noise}}^{\mathrm{DUT}}(\lambda) &= 1 + \frac{u_{\mathrm{noise}}^{\mathrm{DUT}}(\lambda)}{S_2^{\mathrm{DUT}}(\lambda)} \cdot \nu_{\mathrm{noise}}^{\mathrm{DUT}} \end{aligned} \tag{20}$$

for the Monte-Carlo analysis. The random numbers $\nu_{\mathrm{noise}}^{\mathrm{Ref}}$ and $\nu_{\mathrm{noise}}^{\mathrm{DUT}}$ are drawn inside the inner loop of the Monte-Carlo algorithm in order to reflect that noise is uncorrelated with respect to wavelength. Note that in equation (19), $u^2_{S_{\mathrm{bgnd}}^{\mathrm{Ref}}}(\lambda)$ is replaced by $u^2_{S_{\mathrm{dark}}^{\mathrm{Ref}}}(\lambda) + u^2_{S_{\mathrm{stray,ext}}^{\mathrm{Ref}}}(\lambda)$ if a separate measurement of the external stray light is performed as discussed in section 2. In this case, $u_{S_{\mathrm{stray,ext}}^{\mathrm{Ref}}}(\lambda)$ must contain the noise contribution from the additional dark signal measurement for determining $S_{\mathrm{stray,ext}}^{\mathrm{Ref}}(\lambda)$.

3.3.2. Internal background. The dark signal is the residual signal measured by the spectrometer if incident light is completely blocked, e.g. by putting a cap on the measuring head. Some spectrometers feature an internal shutter, which facilitates an automatic dark signal acquisition. The dark signal must be corrected for as outlined in section 2. In general, the magnitude of the dark signal depends on the integration time chosen for the measurement. It may also depend on the wavelength and may show a drift over time. Therefore, it is necessary to perform a dark signal measurement directly before or after measuring the spectral irradiance. A drift in the dark signal between these two measurements will cause a deviation in $S_2^X(\lambda)$ according to equations (4) and (11) and must thus be taken into account in the uncertainty budget.

The drift of the dark signal can be assessed experimentally by a series of consecutive dark signal measurements $S_{\mathrm{dark}}(t_1, t_2, \ldots)$ at different times t_i over a certain time period under typical measurement conditions. From this measurement, the dark signal drift

$$\Delta S_{\mathrm{dark}}(\lambda, t_i) = \frac{S_{\mathrm{dark}}(\lambda, t_i) - S_{\mathrm{dark}}(\lambda, t_{i-1})}{t_i - t_{i-1}} \tag{21}$$

can be calculated. The uncertainty related to the dark signal drift can then be approximated conservatively by

$$u_{\mathrm{dark}}(\lambda) = t_{\mathrm{drift}} \times \max\left(\Delta S_{\mathrm{dark}}(\lambda, t_i)\right)\,, \tag{22}$$

where t_{drift} is the typical time between the measurements of $S_1^X(\lambda)$ and the dark signal $S_{\mathrm{dark}}^X(\lambda)$. In the Monte-Carlo analysis, drifting of the dark signal is then represented by the factors

$$\begin{aligned} f_{\mathrm{dark}}^{\mathrm{Ref}}(\lambda) &= 1 + \frac{u_{\mathrm{dark}}}{S_2^{\mathrm{Ref}}(\lambda)} \cdot \rho_{\mathrm{dark}}^{\mathrm{Ref}}\,, \\ f_{\mathrm{dark}}^{\mathrm{DUT}}(\lambda) &= 1 + \frac{u_{\mathrm{dark}}}{S_2^{\mathrm{DUT}}(\lambda)} \cdot \rho_{\mathrm{dark}}^{\mathrm{DUT}}\,. \end{aligned} \tag{23}$$

Note that using $\max\left(\Delta S_{\mathrm{dark}}(\lambda,t_i)\right)$ is a feasible approach as long as u_{dark} is no limiting contribution in the uncertainty budget, which is usually the case for state-of-the-art spectrometers (compare section 4). Otherwise, more effort may be required for treating this uncertainty contribution, e.g. dark signal measurements before and after the illuminated measurement.

3.3.3. External stray light. External stray light refers to light incident onto the spectrometer's measuring head that does not originate *directly* from the light source but is reflected or scattered in the surrounding. This causes an additional signal $S^{\mathrm{Ref}}_{\mathrm{stray,ext}}(\lambda)$ during the determination of $K(\lambda)$, which is not covered by the known spectral irradiance of the reference lamp and must therefore be corrected according to equation (4). The impact of external stray light can be determined experimentally by placing a beam block in between the light source and the spectrometer's measuring head. The geometry and position of the beam block shall be chosen such that its shadow matches the dimensions of the optically active area of the measuring head. Note that this area does not necessarily coincide with the dimensions of the entrance pupil or diffusor optic.

The beam block method provides a good estimate for external stray light. However, the beam block changes the optical properties of the measurement setup, especially for light which is reflected by objects on the optical axis, such as the rear wall of the room. This results in a remaining uncertainty about external stray light, which could be assessed, for instance, by optical simulations of the measurement setup. An option for the experimental assessment of the remaining uncertainty is a variation of the distance between light source and measuring head, while keeping the distance between light source and beam block constant. Having obtained the uncertainty contribution $u^{\mathrm{Ref}}_{\mathrm{stray,ext}}(\lambda)$, it is included in the Monte-Carlo analysis by

$$f^{\mathrm{Ref}}_{\mathrm{stray,ext}}(\lambda) = 1 + \frac{u^{\mathrm{Ref}}_{\mathrm{stray,ext}}(\lambda)}{S^{\mathrm{Ref}}_{4}(\lambda)} \cdot \rho^{\mathrm{Ref}}_{\mathrm{stray,ext}} \,. \tag{24}$$

Using a random number between -1 and 1 reflects that the correction may overestimate as well as underestimate the external stray light due to misalignment of the shadow on the measuring head. External stray light is only considered for the reference measurement and not for the DUT measurement (compare section 2).

3.3.4. Internal stray light. Light scattering inside the spectrometer may lead to a signal contribution at wavelengths different from that of the incident light. This type of stray light is commonly denoted as *spectral* or *internal* stray light. Internal stray light can lead to deviations in the measured signal [18], especially in measurement regimes of low spectral irradiance. The significance of this effect is a property of the specific spectrometer system and of the measured spectral distribution. Unlike external stray light, internal stray light effects cannot be compensated by the measurement procedure. The impact of internal stray light can be quantified and corrected rigorously if the stray light matrix is known [18, 29]. The stray light matrix, which is a unique property of the spectrometer system, is determined by subsequently illuminating the spectrometer with monochromatic light of several wavelengths and measuring the signal at all other wavelengths. If there is evidence for effects due to spectral stray light, but the effort for a rigorous stray light characterization is too high, approaches for reducing the experimental effort related to the correction and its evaluation [30–33] might be considered or a set of edge filters might be used for estimating the impact of spectral stray light in different wavelength regions.

The implementation and uncertainty analysis of spectral stray light correction according to the widely used method by Zong *et al* [18] has been discussed in [33]. The methodology presented in these references can be applied for performing a stray light correction and determining the uncertainty contributions $u^{\mathrm{Ref}}_{\mathrm{stray,int}}(\lambda)$ and $u^{\mathrm{DUT}}_{\mathrm{stray,int}}(\lambda)$, which are included in the uncertainty budget by

$$f^{\mathrm{Ref}}_{\mathrm{stray,int}}(\lambda) = 1 + \frac{u^{\mathrm{Ref}}_{\mathrm{stray,int}}(\lambda)}{S^{\mathrm{Ref}}_{4}(\lambda)} \cdot \rho^{\mathrm{Ref}}_{\mathrm{stray,int}} \,, \tag{25}$$

$$f^{\mathrm{DUT}}_{\mathrm{stray,int}}(\lambda) = 1 + \frac{u^{\mathrm{DUT}}_{\mathrm{stray,int}}(\lambda)}{S^{\mathrm{DUT}}_{4}(\lambda)} \cdot \rho^{\mathrm{DUT}}_{\mathrm{stray,int}} \,. \tag{26}$$

Note that due to the correlations introduced by the correction [33], the random numbers $\rho^{\mathrm{Ref}}_{\mathrm{stray,int}}$ and $\rho^{\mathrm{DUT}}_{\mathrm{stray,int}}$ are determined in the outer loop of the Monte-Carlo algorithm (see figure 3).

3.3.5. Non-linearity of the detector with respect to irradiance. The uncertainty of non-linearity corrections imposes uncertainty for the spectral irradiance of the DUT. This holds independently from the order of magnitude of the correction and especially if the correction is neglected, i.e. $c_{\mathrm{lin,irr}}(\lambda) \equiv 1$. The uncertainty $u_{\mathrm{lin,irr}}\left(S^{X}_{2}(\lambda)\right)$ of the non-linearity correction follows from experimental uncertainties during the determination of the correction factor (see appendix D for an example). For state-of-the-art spectrometers with negligible non-linearities, it is common not to apply a correction and to use a conservative estimate of maximum non-linearity as uncertainty $u_{\mathrm{lin,irr}}(S^{X}_{2})$, where the wavelength dependence is neglected for reasons of simplicity (see section 4 for an example). Having determined the uncertainty of the correction, we take it into account in the Monte-Carlo analysis by the factors

$$\begin{aligned} f^{\mathrm{Ref}}_{\mathrm{lin,irr}}(\lambda) &= 1 + \frac{u_{\mathrm{lin,irr}}\left(S^{\mathrm{Ref}}_{2}(\lambda)\right)}{c_{\mathrm{lin,irr}}\left(S^{\mathrm{Ref}}_{2}(\lambda)\right)} \cdot \rho_{\mathrm{lin,irr}} \,, \\ f^{\mathrm{DUT}}_{\mathrm{lin,irr}}(\lambda) &= 1 + \frac{u_{\mathrm{lin,irr}}\left(S^{\mathrm{DUT}}_{2}(\lambda)\right)}{c_{\mathrm{lin,irr}}\left(S^{\mathrm{DUT}}_{2}(\lambda)\right)} \cdot \rho_{\mathrm{lin,irr}} \,. \end{aligned} \tag{27}$$

Non-linearities are a property of the spectrometer and affect both reference and DUT measurement in the same way. This is reflected by using the same random number $\rho_{\mathrm{lin,irr}}$ for both measurements. Since non-linearities with respect to irradiance are assumed to affect the measured signal in the same way at all

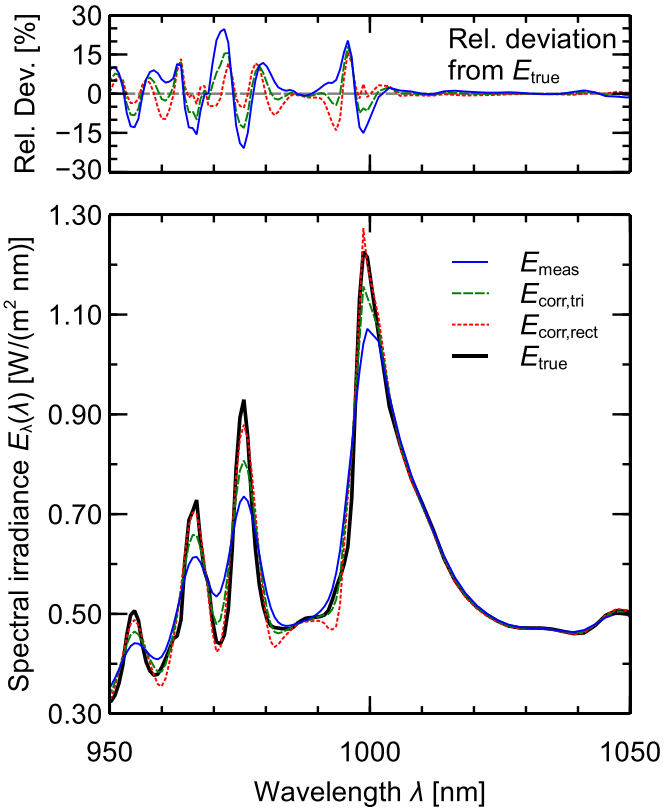

Figure 4. Impact of the bandwidth correction on a simulated spectral irradiance (E_{true}, black solid line) with strong spike features as present in Xenon lamps.

wavelengths, the random number $\rho_{\text{lin,irr}}$ is drawn in the outer loop of the Monte-Carlo algorithm.

3.3.6. Non-linearity of the detector with respect to integration time. Non-linearities with respect to integration time are treated similarly to the previous subsection. The uncertainty $u_{\text{lin,tint}}\left(S^X{}_2(\lambda)\right)$ of the non-linearity correction follows from experimental uncertainties during the determination of the correction factor. For state-of-the-art spectrometers, the correction can often be neglected ($c_{\text{lin,tint}} \equiv 1$) and a maximum non-linearity can be used as uncertainty $u_{\text{lin,irr}}(S^X{}_2)$, where the wavelength dependence is neglected for reasons of simplicity. The uncertainty is then taken into account in the Monte-Carlo analysis by the factors

$$\begin{aligned} f^{\text{Ref}}_{\text{lin,tint}}(t^{\text{Ref}}_{\text{int}},\lambda) &= 1+\frac{u_{\text{lin,tint}}\left(t^{\text{Ref}}_{\text{int}},\lambda\right)}{c_{\text{lin,tint}}\left(t^{\text{Ref}}_{\text{int}},\lambda\right)}\cdot\rho_{\text{lin,tint}}\,, \\ f^{\text{DUT}}_{\text{lin,tint}}(t^{\text{DUT}}_{\text{int}},\lambda) &= 1+\frac{u_{\text{lin,tint}}\left(t^{\text{DUT}}_{\text{int}},\lambda\right)}{c_{\text{lin,tint}}\left(t^{\text{DUT}}_{\text{int}},\lambda\right)}\cdot\rho_{\text{lin,tint}}\,. \end{aligned} \tag{28}$$

3.3.7. Spectral bandwidth. The spectral bandwidth $\Delta\lambda$ of a monochromator characterizes the wavelength interval $[\lambda-\Delta\lambda/2,\,\lambda+\Delta\lambda/2]$ around the nominal wavelength λ, within which the transmittance is greater then zero. It is determined, for instance, by the geometry of the grating and the slit width. Typically, it depends on the wavelength. Array spectrometers often feature a spectral bandwidth that exceeds the spectral sampling, meaning that sharp spectral lines are detected by several pixels.

Spectral bandwidth generates an additional detector signal $S_{\text{bw}}(\lambda)$ due to light incident at adjacent wavelengths and leads to a broadening of sharp spectral features, as illustrated in figure 4. This figure shows a simulated spectral irradiance (E_{true}, black solid line) with strong spike features as present, for instance, in Xenon lamps. The blue curve E_{meas} represents the measured spectral irradiance. It is calculated by folding E_{true} with a triangular slit function with $\Delta\lambda = 10$ nm. The green and red curves show the results of the application of two different bandwidth corrections (assuming a triangular and rectangular slit function, respectively) to the blue curve in order to reconstruct E_{true} out of E_{meas}. For the correction, we use the analytical formula equation (8). A derivation of the formula is given in appendix E. Figure 4 demonstrates that this correction restores the sharp spectral features, but also leads to some falsification, especially in the valleys between the sharp spectral features. In some cases, the correction may also enhance statistical noise.

The spectral bandwidth correction according to equation (8) assumes a triangular bandpass function, which holds for an ideal monochromator [34]. However, real spectrometers usually feature a bandpass function that is rather gaussian-shaped or even almost rectangular. The exact shape of the bandpass function is often unknown, especially for array spectrometers. Gaussian or rectangular bandpass functions lead to an increased signal $S_{\text{bw}}(\lambda)$ compared to a triangular bandpass function and hence require a modified correction function (see appendix E). Furthermore, the proposed spectral bandwidth correction formula only takes adjacent data points into account. This mathematical simplification is, strictly speaking, only applicable for spectral bandwidths that are approximately of the same order of magnitude as the spectral sampling, which is often not the case for the spectrometers used throughout the laboratories. For uncertainty treatment using Monte-Carlo methods, we therefore propose to randomly vary around the triangular bandpass correction (ideal case) between no bandwidth correction (delta-shaped bandpass function) and correction using a rectangular bandpass function (worst case). In figure 4, this would lead to corrected spectral irradiance curves lying between the blue curve (measured data) and the red curve (corrected for a rectangular bandpass function). We choose the distribution function of the corresponding random number to be triangular. This reflects that the actual bandpass function is most probably located somewhere around the triangular bandpass function, whereas the probability for having a delta-shaped or rectangular bandpass function is zero. For a rectangular bandpass function, the correction function is twice the correction function for a triangular bandpass function (see appendix E). Hence, the variation between no correction and rectangular bandpass correction can be included in the Monte-Carlo analysis by the factors

$$\begin{aligned} f^{\text{Ref}}_{\text{bw}}(\Delta\lambda,\lambda) &= 1+\Big(c_{\text{bw}}(\Delta\lambda,\lambda)-1\Big)\cdot\tau_{\text{bw}}\,, \\ f^{\text{DUT}}_{\text{bw}}(\Delta\lambda,\lambda) &= 1+\Big(c_{\text{bw}}(\Delta\lambda,\lambda)-1\Big)\cdot\tau_{\text{bw}}\,. \end{aligned} \tag{29}$$

Note that $S_{\mathrm{bw}}(\lambda)$ is correlated between reference and DUT measurement, which is reflected in the Monte-Carlo analysis by using the same random number τ_{bw} for both $f_{\mathrm{bw}}^{\mathrm{Ref}}(\lambda)$ and $f_{\mathrm{bw}}^{\mathrm{DUT}}(\lambda)$.

3.3.8. Wavelength accuracy. In order to obtain the spectrometer signal as a function of wavelength λ, the relation between grating position and selected wavelength of the monochromator (or pixel number and wavelength for array spectrometers, respectively) must be established. This is usually achieved by using spectral calibration lamps. These spectral calibration lamps produce narrow, intense lines of ultraviolet (UV) to infrared (IR) wavelengths due to the excitation of various rare gases and metal vapors, for which the wavelength is known [35, 36]. Since only a limited number of spectral lines is available for the wavelength calibration, a parametrization function is usually fitted to the measured data. For grating monochromators, linear functions are often sufficient, whereas for array spectrometers, higher-order polynomials are frequently used.

From the wavelength calibration, a wavelength uncertainty $u_{\mathrm{wl}}(\lambda)$ can be derived, which depends on the wavelength in general. Basically, there are two options for dealing with the wavelength uncertainty within the Monte-Carlo analysis: First, the wavelength scale can be changed according to $u_{\mathrm{wl}}(\lambda)$ in each Monte-Carlo iteration. Afterwards, the resulting signals are interpolated to specific grid points (e.g. the nominal wavelengths of the signals $S^X(\lambda)$) in order to enable the calculation of $E_{\lambda,i}^{\mathrm{DUT}}(\lambda)$ and its distribution. This approach is a rigorous treatment of wavelength calibration uncertainties; however, by changing the wavelength scale on each Monte-Carlo iteration, complexity is added to the evaluation. The second option is propagating the wavelength uncertainty $u_{\mathrm{wl}}(\lambda)$ to a change of the signals $S^X(\lambda)$. This can be done, for instance, by calculating the slope

$$s^X(\lambda_i) = \frac{\partial S^X(\lambda)}{\partial \lambda}\Big|_{\lambda_i} \approx \frac{S^X(\lambda_{i+1}) - S^X(\lambda_{i-1})}{\lambda_{i+1} - \lambda_{i-1}} \tag{30}$$

of the curve. The right hand side of the latter equation represents a numeric approximation of the derivative for discrete data. The maximum signal change due to wavelength deviations is then

$$\Delta S_{\mathrm{wl}}^X(\lambda) \approx s^X(\lambda)\, u_{\mathrm{wl}}(\lambda) \tag{31}$$

and the uncertainty of the wavelength calibration is included in the Monte-Carlo analysis using the factors

$$\begin{aligned} f_{\mathrm{wl}}^{\mathrm{Ref}}(\lambda) &= 1 + \frac{\Delta S_{\mathrm{wl}}^{\mathrm{Ref}}(\lambda)}{S_4^{\mathrm{Ref}}(\lambda)} \cdot \rho_{\mathrm{wl}}\,, \\ f_{\mathrm{wl}}^{\mathrm{DUT}}(\lambda) &= 1 + \frac{\Delta S_{\mathrm{wl}}^{\mathrm{DUT}}(\lambda)}{S_4^{\mathrm{DUT}}(\lambda)} \cdot \rho_{\mathrm{wl}}\,. \end{aligned} \tag{32}$$

This approach is used in our application example presented in the next section. Note that correlations between reference and DUT measurement are reflected by using the same random number ρ_{wl} for both factors. Also note that ρ_{wl} is determined in the outer loop of the Monte-Carlo algorithm because we assume that a misalignment of the grating (or the pixel number-to-wavelength relation for array spectrometers, respectively) affects both reference and DUT measurement in the same way. This assumption is usually justified. However, there may be situations where a different treatment is necessary, e.g. if there are movable components inside the spectrometer that affect the wavelength scale and cannot be positioned reproducibly or move upon changes of the device temperature.

3.3.9. Spectral irradiance of reference lamp. The uncertainty of the spectral irradiance $E_\lambda^{\mathrm{Ref}}(\lambda)$ of the reference lamp is taken from its calibration certificate. The values given there usually refer to a coverage factor $k = 2$ and a normal distribution. Hence, the uncertainty $u_{\mathrm{E^{Ref}}}(\lambda)$ is obtained by dividing these values by 2. We include the uncertainty of $E_\lambda^{\mathrm{Ref}}(\lambda)$ in our analysis with the factor

$$f_{\mathrm{Eref}}(\lambda) = 1 + \frac{u_{\mathrm{E^{Ref}}}(\lambda)}{E_\lambda^{\mathrm{Ref}}(\lambda)} \cdot \nu_{\mathrm{E^{Ref}}}\,. \tag{33}$$

If the calibration certificate states relative uncertainties, which is often the case, the division with $E_\lambda^{\mathrm{Ref}}(\lambda)$ has to be omitted. The point of determination of the random number $\nu_{\mathrm{E^{Ref}}}$ within the Monte-Carlo algorithm depends on whether $E_\lambda^{\mathrm{Ref}}(\lambda)$ is correlated with respect to wavelength or not. In the first case, $\nu_{\mathrm{E^{Ref}}}$ is determined in the outer loop; in the second case, it is determined in the inner loop. Partial correlations can be considered by using the value of an additional random number for deciding whether to use correlation or no correlation in each Monte-Carlo cycle. In general, information about wavelength correlations of $E_\lambda^{\mathrm{Ref}}(\lambda)$ needs to be provided by the calibration institution in order to account for them properly in the uncertainty analysis.

3.3.10. Distance adjustment. The uncertainty of the distance adjustment u_{dist} is determined by two components: The uncertainty of the distance measurement and the uncertainty of the distance offset correction factor c_{dist}. The uncertainty of the distance measurement depends on the accuracy of the measuring instrument (e.g. a micrometer gauge), which can be obtained from its calibration certificate, and the alignment accuracy of the measuring instrument. The alignment uncertainty can often only be estimated and is usually larger than the uncertainty of the instrument's calibration. For measuring heads with $\Delta d > 0$, however, the uncertainty of Δd is often the dominant contribution to u_{dist}. One option for the determination of this uncertainty component is performing a Monte-Carlo analysis for the evaluation of Δd according to equation (B5). Afterwards, all uncertainty components can be combined into u_{dist} using the standard GUM formalism.

In order to take u_{dist} into account for the uncertainty budget of $E_\lambda^{\mathrm{DUT}}(\lambda)$, we model the impact of distance variations using the inverse square law for point light sources,

$$E(d) = \frac{I}{d^2}\,, \tag{34}$$

where I denotes (spectral) radiant intensity directly at the light source. If a small deviation δd from d occurs, Taylor series expansion of equation (34) around d yields

$$E(d+\delta d) \approx E(d)\left(1-\frac{2\,\delta d}{d}\right). \tag{35}$$

In the Monte-Carlo analysis, δd is calculated on each iteration according to $\delta d = u_{\mathrm{dist}} \cdot \rho_{\mathrm{dist}}$, where u_{dist} defines the maximum deviation from d according to the analysis described above. Inserting this relation into the latter equation, we obtain the distance correction factor

$$f_{\mathrm{dist}} = 1 - \frac{2\,u_{\mathrm{dist}}}{d} \cdot \rho_{\mathrm{dist}} \tag{36}$$

for use in the Monte-Carlo analysis. This correction factor is not wavelength dependent. The random number ρ_{dist} is therefore drawn in the outer loop of the Monte-Carlo algorithm. Note that the uncertainty of Δd as resulting from the Monte-Carlo analysis may be normally distributed. If this is the dominant component of u_{dist}, f_{dist} should be calculated using a normally distributed random number ν_{dist} instead of ρ_{dist}. Also, note that there are measuring heads that feature a wavelength-dependent offset, which may require a different treatment.

3.3.11. Accuracy of lamp operating current. The spectral irradiance $E_\lambda^{\mathrm{Ref}}(\lambda)$ of the reference lamp is given for a specific operating current, at which the lamp must be operated. Any deviations from this nominal current lead to a change of the temperature of the filament, which in turn leads to a deviation of the spectral irradiance $E_\lambda^{\mathrm{Ref}}(\lambda)$ from the values tabulated in the calibration certificate.

In order to estimate the change in $E_\lambda^{\mathrm{Ref}}(\lambda)$ due to operating current variations, we model the reference lamp as a black body radiator with the spectral irradiance [37]

$$E_{\mathrm{bb}}(\lambda,T) \propto \frac{hc}{\lambda^5}\left[\exp\left(\frac{hc}{\lambda k T}\right)-1\right]^{-1}, \tag{37}$$

where h denotes the Planck constant, c the speed of light in vacuum, k the Boltzmann constant and T the temperature of the filament (in units of Kelvin). In section 4, the validity of this approach is demonstrated. The operating temperature T_{op} of the filament is estimated using the linear approximation

$$R(T_{\mathrm{op}}) = R_0\big(1+\alpha(T_{\mathrm{op}}-T_0)\big) \tag{38}$$

for the resistance R of the filament, which can be solved for T_{op}. In the latter equation, R_0 denotes the resistance at room temperature T_0 and α is the temperature coefficient of the filament, which can be taken from literature. The resistance R_0 at room temperature can be determined with a multimeter, whereas the resistance $R(T_{\mathrm{op}})$ at operating temperature is approximated from voltage and current measurements at the terminals of the lamp during operation at the nominal voltage V_{op} and current I_{op} using Ohm's law:

$$R(T_{\mathrm{op}}) = \frac{V_{\mathrm{op}}}{I_{\mathrm{op}}}. \tag{39}$$

Laboratories usually perform these measurements anyway in order to monitor the temporal stability of the lamp. The dependence of the filament temperature on small variations δI of the operating current can be calculated approximately by combining equation (39) and equation (38), solving for T and performing a Taylor series expansion around T_{op}. This yields

$$T \approx T_{\mathrm{op}} - \delta T, \tag{40}$$

where

$$T_{\mathrm{op}} = \frac{V_{\mathrm{op}} + I_{\mathrm{op}} R_0 (T_0\alpha - 1)}{I_{\mathrm{op}} R_0 \alpha}, \tag{41}$$

$$\delta T = \frac{V_{\mathrm{op}}}{I_{\mathrm{op}}^2 R_0 \alpha} \cdot \delta I. \tag{42}$$

With equations (37) through (42), the change of the spectral irradiance is

$$\delta E_{\mathrm{bb}}(\lambda, T_{\mathrm{op}}, \delta T) = E_{\mathrm{bb}}(\lambda, T_{\mathrm{op}} \pm \delta T) - E_{\mathrm{bb}}(\lambda, T_{\mathrm{op}}). \tag{43}$$

In the Monte-Carlo analysis, δI is calculated on each iteration according to $\delta I = u_{\mathrm{cur}} \cdot \rho_{\mathrm{curr}}$, where u_{cur} is the uncertainty of the current measurement, i.e. defines the maximum deviation from I_{op}. It must be determined by a separate uncertainty analysis and depends on the instrumentation for operating the lamp. In summary, the temperature variation on each Monte-Carlo iteration is

$$\delta T = \frac{V_{\mathrm{op}}}{I_{\mathrm{op}}^2 R_0 \alpha} \cdot u_{\mathrm{cur}} \rho_{\mathrm{curr}} \tag{44}$$

and we obtain a factor

$$f_{\mathrm{cur}}(\lambda) = 1 + \frac{\delta E_{\mathrm{bb}}(\lambda, T_{\mathrm{op}}, \delta T)}{E_{\mathrm{bb}}(\lambda, T_{\mathrm{op}})} \tag{45}$$

for use in the Monte-Carlo analysis. Note that we assume a rectangular distribution for δI because the measurement uncertainty of the multimeter, which is rectangularly distributed, is usually the dominant uncertainty component. A different treatment might be necessary if δI is not rectangularly distributed. The random number ρ_{curr} is determined in the outer loop of the Monte-Carlo analysis in order to reflect that variations of the operating current cause correlations with respect to wavelength in the measured spectral irradiance.

Another possibility for quantifying the uncertainty related to the lamp operating current is measuring the signal $S_5^{\mathrm{Ref}}(\lambda)$ while tuning the operating current close to its nominal value I_{op}. Thereby, the factor

$$f_{\mathrm{cur}}(\lambda) = 1 + \frac{u_{\mathrm{cur}}}{S_5^{\mathrm{Ref}}(\lambda)} \left.\frac{\partial S_5^{\mathrm{Ref}}(\lambda)}{\partial I}\right|_{I_{\mathrm{op}}} \cdot \rho_{\mathrm{curr}}. \tag{46}$$

can be determined experimentally.

3.3.12. Long term reproducibility. Uncertainty contributions that lead to deviations in the radiometric correction function $K(\lambda)$ over time are summed into this contribution. This covers, for instance, aging effects of the instrument, mechanical instabilities that may result from transport or storage and possibly non-reproducible instrument settings such as fibre connections. Moreover, ageing of the reference lamp is covered by this contribution. Ageing of reference lamps is discussed in more detail in appendix A. Deviations of the radiometric correction function can be evaluated experimentally, for instance, by comparing different measurements of the radiometric correction function over time, which are performed under the same conditions and with an identical setup. From these data, the mean radiometric correction function $\overline{K}(\lambda)$ and its uncertainty $u_{\mathrm{rep}}(\lambda)$ can be calculated. This uncertainty contribution is then taken into account in the uncertainty budget by the factor

$$f_{\mathrm{rep}}(\lambda) = 1 + \frac{u_{\mathrm{rep}}(\lambda)}{\overline{K}(\lambda)} \cdot \rho_{\mathrm{rep}} \,. \tag{47}$$

3.3.13. Temperature effects. Temperature dependent properties of several spectrometer components can affect the measured signal. For instance, the spectral responsivity of the detector can have a wavelength dependent temperature coefficient. Moreover, mechanical parts in the spectrometer (such as slits or optical gratings) could move upon temperature variations and thereby affect the measured signal. Changes of the instrument's temperature can arise not only from changes of the ambient temperature, but also from radiative heating by the light source or from internal heating caused by the electronics. For this reason, state-of-the-art spectrometers often feature temperature-controlled detectors. If temperature affects the measured signal, a correction is required as outlined in section 2 and appendix C. The uncertainty u_{temp} of this correction, which follows from experimental uncertainties during the determination of the temperature correction factor c_{temp}, imposes uncertainty for the spectral irradiance of the DUT (see section 4 for an example). This also holds if the correction is neglected (i.e. $c_{\mathrm{temp}} \equiv 1$). Having determined the uncertainty of the correction factor, we take it into account in the Monte-Carlo analysis by the factor

$$f_{\mathrm{temp}}(\lambda) = 1 + \frac{u_{\mathrm{temp}}(\lambda)}{c_{\mathrm{temp}}(\lambda)} \cdot \rho_{\mathrm{temp}} \,. \tag{48}$$

The random number ρ_{temp} is determined in the outer loop of the Monte-Carlo algorithm because we assume that changes of the temperature affect the measurement in the same way at all wavelengths. This usually holds for array spectrometers, which are widely used throughout the laboratories. For slow scanning spectrometers, a different treatment might be necessary.

3.3.14. Tilt of the measuring head. For the measurements, the measuring head needs to be adjusted such that the optical axis runs perpendicularly through its center, i.e. the angle θ between its surface normal and the optical axis is 0. Any deviation from $\theta = 0$ will lead to deviations of the signal $S_5^X(\lambda)$. The uncertainty u_{tilt}^X of the angle adjustment can be estimated, for instance, by using a laser beam which is adjusted parallely to the optical axis and irradiates the measuring head from a large distance. From the lateral displacement of the reflected beam, the tilt angle can then be calculated using trigonometrical relations.

In order to model the impact of tilt on the spectrometer signal, we note that in the vicinity of $\theta = 0$, the angular response of typical measuring heads can be described by the cosine relation

$$\frac{S(\theta)}{S_0} = \cos\theta \,, \tag{49}$$

where S_0 is the signal under perpendicular incidence of light. If a small deviation $\delta\theta$ from 0 occurs, Taylor series expansion of the latter equation around 0 yields

$$\frac{S(\delta\theta)}{S_0} \approx 1 - \delta\theta^2/2 \,. \tag{50}$$

In the Monte-Carlo analysis, $\delta\theta$ is calculated on each iteration according to $\delta\theta = u_{\mathrm{tilt}}^X \cdot \rho_{\mathrm{tilt}}^X$. Inserting this into the latter equation, we obtain the factors

$$\begin{aligned} f_{\mathrm{tilt}}^{\mathrm{Ref}} &= 1 - \frac{(u_{\mathrm{tilt}}^{\mathrm{Ref}})^2}{2} \cdot \rho_{\mathrm{tilt}}^{\mathrm{Ref}} \,, \\ f_{\mathrm{tilt}}^{\mathrm{DUT}} &= 1 - \frac{(u_{\mathrm{tilt}}^{\mathrm{DUT}})^2}{2} \cdot \rho_{\mathrm{tilt}}^{\mathrm{DUT}} \,. \end{aligned} \tag{51}$$

for use in the Monte-Carlo analysis. These factors are not wavelength dependent because we assume that $\delta\theta$ affects the signal in the same way at all wavelengths. This assumption is approximately fulfilled for typical measuring heads. The random numbers $\rho_{\mathrm{tilt}}^{\mathrm{Ref}}$ and $\rho_{\mathrm{tilt}}^{\mathrm{DUT}}$ are therefore determined in the outer loop of the Monte-Carlo analysis. Note that $\delta\theta$ and u_{tilt}^X are specified in units of radians here.

3.3.15. Non-uniformity of the light field and temporal stability of the DUT. The spectral irradiance of the DUT is determined at a position (x_0, y_0) in the light field at a certain point t_0 in time. Spatial and temporal variations of the spectral irradiance may lead to deviations if the measurement position is changed or if the measurement is repeated at a later point in time. It depends on the purpose of the measurement whether these contributions should be considered or not. If the intention of the measurement is the determination of the spectral irradiance 'as is' at the moment and position of measurement, they can be ignored. If the intention is a comparison between different instruments that do not measure simultaneously or not at the same position, these uncertainty contributions should be included. They could be estimated experimentally by carrying out measurements of $S_4^{\mathrm{DUT}}(\lambda)$ at different positions in the light field (giving $u_{\mathrm{non-u}}^{\mathrm{DUT}}(\lambda)$) and/or at different points in time (giving $u_{\mathrm{stab-t}}^{\mathrm{DUT}}(\lambda)$). From these measurements, correction factors

$$f_{\mathrm{non-u}}^{\mathrm{DUT}}(\lambda) = 1 + \frac{u_{\mathrm{non-u}}^{\mathrm{DUT}}(\lambda)}{S_4^{\mathrm{DUT}}(\lambda)} \cdot \rho_{\mathrm{non-u}}^{\mathrm{DUT}} \,, \tag{52}$$

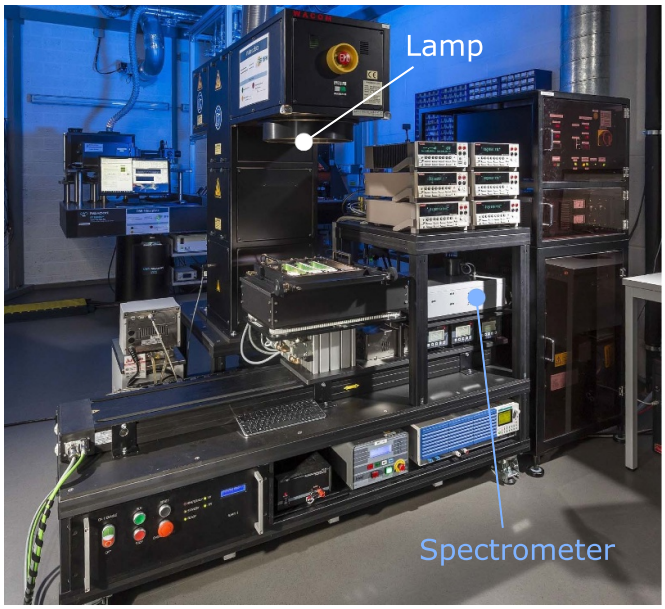

Figure 5. ISFH CalTeC's current-voltage characteristic measurement facility for solar cells. The solar simulator (WACOM WXS-156 S-L2) provides a light field of 170 × 170 mm^2.

$$f^{\mathrm{DUT}}_{\mathrm{stab-t}}(\lambda) \quad = \quad 1 + \frac{u^{\mathrm{DUT}}_{\mathrm{stab-t}}(\lambda)}{S^{\mathrm{DUT}}_{4}(\lambda)} \cdot \rho^{\mathrm{DUT}}_{\mathrm{stab-t}} \qquad (53)$$

can be obtained. $f^{\mathrm{DUT}}_{\mathrm{non-u}}(\lambda)$ is especially important for large-area solar simulators and $f^{\mathrm{DUT}}_{\mathrm{stab-t}}(\lambda)$ is especially important for pulsed solar simulators. The spectral irradiance of a pulsed solar simulator can vary during ignition, on the plateau and during the decay phase of the pulse. Such variations can be evaluated by measuring the spectral irradiance with a spectroradiometer featuring an integration time much smaller than the pulse duration. Furthermore, the reproducibility of such measurements should be carefully evaluated.

4. Application example

As an application example, we specifically describe the procedure for determining the spectral irradiance of ISFH CalTeC's solar simulator, which is used for certified measurements of solar cells. The solar simulator forms part of a current-voltage characteristic (IV) measuring facility, which is shown in figure 5. It is a two lamp system (Xenon and Halogen) from WACOM (WXS-156 S-L2) and produces a spectral irradiance similar to the AM1.5G distribution as tabulated in the IEC 60 904-3 standard [38]. The size of the quadratic light-field is 170 × 170 mm^2. The solar simulator is rated as AAA (rating for: spectral match to AM1.5G, non-uniformity of irradiance and instability of irradiance) according to the IEC60 904-9 standard [39]. For a convenient and fast determination of the spectral irradiance, an array spectrometer (see next section) is integrated on a motorized stage.

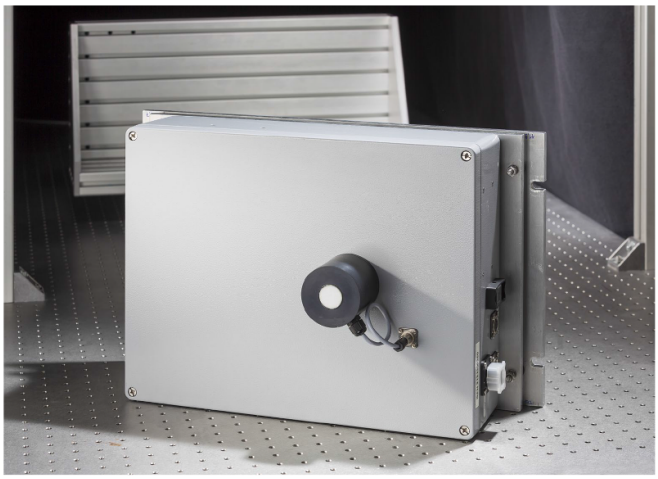

Figure 6. *CompactSpec* spectrometer (demounted from the IV measuring facility) used for measuring the spectral irradiance of the solar simulator.

4.1. Instrumentation and measurement procedure

The spectral irradiance of the solar simulator is acquired for each solar cell calibration measurement and thus very often. In order to achieve short measurement times of the order of seconds, we use a custom-made *CompactSpec* array spectrometer manufactured by tec5, which is shown in figure 6. The spectrometer features a silicon array detector (Zeiss, MCS 55 UV-NIR) and an indium gallium arsenide array detector (Zeiss, PGS-NIR 1,7) and is sensitive in the wavelength range from 200 nm to 1700 nm. As can be seen in the picture, the measuring head of the instrument (transmission diffuser) is attached to the housing in order to avoid problems with moving optical fibers. At the IV measurement facility, the spectrometer is mounted on a motorized stage, which allows to move it into the light field of the solar simulator automatically as shown in figure 5. The measuring head of the spectrometer is equipped with a software-controllable optical shutter. The InGaAs detector is temperature-controlled. The Si-CCD detector does not feature a temperature control. However, a Pt1000 temperature sensor is attached to the detector in order to monitor its temperature, which is used as input for a temperature correction as described in the next section. A spectral stray light correction matrix according to the method by Zong *et al* [18] was determined for the instrument using the PLACOS facility at PTB [40] upgraded with a new nanosecond-OPO operating at 1 kHz repetition rate. The spectral stray light correction and its uncertainty have been discussed in detail in [33].

A schematic of the calibration facility for our spectrometer is shown in figure 7. The facility consists of an optical table with an area of 100 × 300 cm^2, on which the components are mounted. The reference lamp is mounted on a lamp holder, which can be adjusted using a y-z-φ stage. We use 250 W quartz tungsten halogen (QTH) lamps, usually of the types BN-LH250-BC (Gigahertz Optik) or HLX 64 654 (Osram). The spectral irradiance of these lamps is calibrated at the PTB. Figure 8 depicts the typical spectral irradiance of a reference

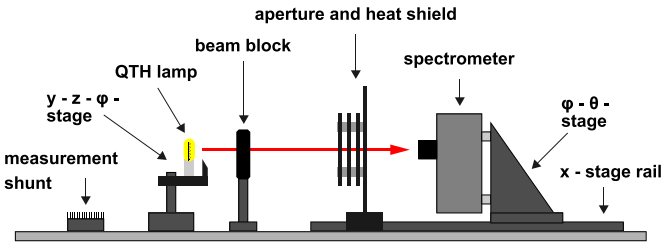

Figure 7. Schematic of the measurement facility for determining the radiometric correction function $K(\lambda)$ of spectrometers at ISFH CalTeC. The housing made of black molton fabric is not shown in the figure.

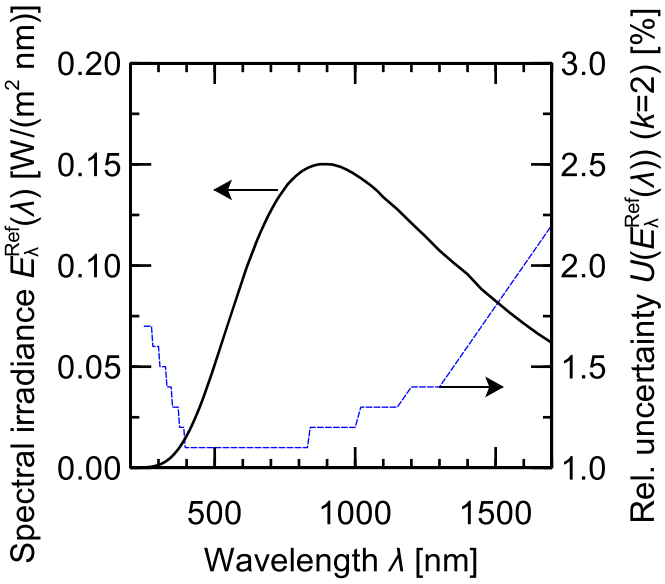

Figure 8. Typical spectral irradiance of a reference lamp (250 W QTH lamp) at a distance of 300 mm and corresponding uncertainty ($k = 2$) as given by PTB.

lamp at a distance of 300 mm and the corresponding measurement uncertainty ($k = 2$). Using 250 W lamps instead of 1000 W FEL lamps (the common type of reference lamp in many laboratories) is advantageous with respect to limited space in our laboratory because the measurement facility can be constructed more compact and the heat input into the room is reduced. On the other hand, the shorter measuring distance requires a more accurate distance adjustment. Between the reference lamp and the measuring head of the spectrometer, an aperture and a beam block are positioned. The beam block (width 15 mm) is motorized to carry out automatic background signal measurements.

The lamp is operated by a precision power supply (Heinzinger, PTNhp 125-10) which is capable of providing the lamp operating current I_{op} of 9.7A with a deviation of not more than ± 0.7 mA (0.007%) according to our measurement uncertainty analysis. Two multimeters (Fluke 8845A) are used for measuring the lamp operating voltage V_{op} directly at the terminals and the voltage drop over the measurement shunt (Isabellenhütte, RUG-Z-R100-0.1-TK10) to determine the lamp current I_{op}. The measurement shunt is connected in series to the lamp

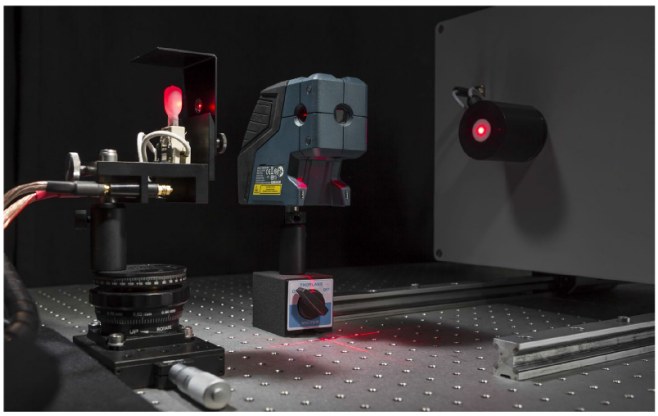

Figure 9. Alignment of reference lamp and measuring head on the optical axis using the bidirectional alignment laser.

and the power supply. It is attached to the table for cooling purposes. During the operation of the lamp, the computer continuously monitors operating voltage, current and power $P_{op} = V_{op} \cdot I_{op}$ as well as the temperature of the measurement shunt. The shunt temperature is monitored using a Pt1000 temperature sensor, which is attached to the shunt and connected to a ZILA DTM5080 measurement controller plugged to the computer. We consider the lamps stable if the operating power does not vary by more than 0.5 W after calibration. This threshold value results from the analysis outlined in appendix A.

The spectrometer is mounted on an x-stage rail, such that the distance between the reference lamp and the detector head can be precisely adjusted. For this purpose, we use an inside micrometer gauge (Mitutoyo, 339-301) with an accuracy of ± 1 µm. Thereby, we are able to adjust the distance with an accuracy of ± 100 µm. This value follows from the uncertainty of the length calibration and the reproducibility of the distance adjustment. The precise alignment of the reference lamp and the measuring head of the spectrometer on the optical axis is facilitated by a bidirectional alignment laser (Bosch GPL5C Professional), which is placed in between the lamp and the detector head (see figure 9).

The nominal distance, for which the spectral irradiance of our 250 W QTH reference lamps is specified in the calibration certificate, is 300 mm. According to a distance variation measurement as described in appendix B, the offset of the spectrometer's measuring head is determined to be (1.96 ± 0.78) mm. We thus set the micrometer gauge to 298.04 mm (compare figure 1) and take the uncertainty of this correction plus the uncertainty of the distance adjustment (100 µm) into account as u_{dist}.

After a sufficient warm-up time for the spectrometer electronics (2 h) and the reference lamps (20 min), the radiometric correction function $K(\lambda)$ of the spectrometer is determined by relating the detector signal to the known spectral irradiance of the reference lamp as described in section 2. We apply the corrections mentioned there and repeat the measurement 25 times. External stray light and detector dark signal are measured simultaneously by moving the beam block into the beam path. The overall measurement time is of the order of 50 s. Since drifting

Table 1. Input parameters for the uncertainty analysis.

Parameter	Si detector	InGaAs detector
u_{dark}	$9.865 \times 10^{-6}\ \mathrm{s}^{-1}$	$5.733 \times 10^{-7}\ \mathrm{s}^{-1}$
$u_{\mathrm{stray,ext}}$	5.5×10^{-4}	5.5×10^{-4}
$u_{\mathrm{lin,tint}}$	6.785×10^{-4}	1.809×10^{-4}
$u_{\mathrm{lin,irr}}$	4.536×10^{-4}	3.163×10^{-3}
$\Delta\lambda$	3.5 nm	7 nm
u_{wl}	0.15 nm	0.15 nm
u_{cur}	0.7 mA	0.7 mA
u_{rep}	4.374×10^{-3}	1.951×10^{-3}
u_{dist}	0.88 mm	0.88 mm
u^{X}_{tilt}	0.01 rad	0.01 rad
u_{temp}	0.3 °C	0.3 °C
u^{X}_{noise}	standard deviation of 25 repeated measurements	
$u_{\mathrm{temp}} \cdot c_{\mathrm{T}}(\lambda)$	see figure 10	
$u^{\mathrm{Ref}}_{\mathrm{stray,int}}(\lambda)$	see figure 10	
$u^{\mathrm{DUT}}_{\mathrm{stray,int}}(\lambda)$	see figure 10	
$u_{\mathrm{E^{Ref}}}(\lambda)$	see figure 10	

of the dark signal is negligible on this time scale, we are able to apply a sequential measurement mode (25 sequential measurements without beam block, afterwards 25 measurements with beam block). For convenience, we store the resulting $K(\lambda)$ in a file that is loaded and directly applied in the software controlling the IV measurement facility. The radiometric correction function of our instrument is stable on time scales of months. A recalibration is performed every six months. Additionally, the stability is routinely checked in between the recalibrations using a field calibrator light source (CMS Schreder, KS-J1011), which can be used without demounting the spectrometer from the IV measurement facility.

4.2. Measurement uncertainty evaluation

This section summarizes the experimental determination of the parameters used for the measurement uncertainty analysis according to the methodology outlined in section 3. The resulting values are listed in table 1 and figure 10.

4.2.1. Measurement noise. is taken into account by repeating all measurements 25 times and using mean values and standard deviations for the calculations.

4.2.2. Drift of the dark signal. This uncertainty contribution is experimentally determined from a series of dark signal measurements over the course of several hours under typical measurement conditions. From these data, the maximum drift $\Delta S_{\mathrm{dark}}(\lambda)$ is obtained and multiplied with the typical time between illuminated and dark measurements (50 s).

4.2.3. External stray light. We estimate the efficiency of the external stray light correction (beam block method) in our setup by ray tracing simulations using the ray tracer DAIDALOS [41]. The simulation allows to distinguish between *direct* light rays from the light source and *indirect* rays, i.e. rays that undergo at least one reflection within the setup before hitting the measuring head and thus represent external stray light. Hence, the simulation allows to investigate deviations of the the measured signal S_{meas} with external stray light correction from the ideal signal S_{id} (only direct rays). From the simulation, we deduce a *relative* uncertainty of $S_4^{\mathrm{Ref}}(\lambda)$ of

$$u^{\mathrm{Ref}}_{\mathrm{stray,ext}} = 0.0005 \tag{54}$$

for all wavelengths, which we include in the Monte-Carlo analysis using the factor

$$f^{\mathrm{Ref}}_{\mathrm{stray,ext}} = 1 + u^{\mathrm{Ref}}_{\mathrm{stray,ext}} \cdot \rho^{\mathrm{Ref}}_{\mathrm{stray,ext}} \cdot \tag{55}$$

Details about the ray tracing simulation are given in appendix F.

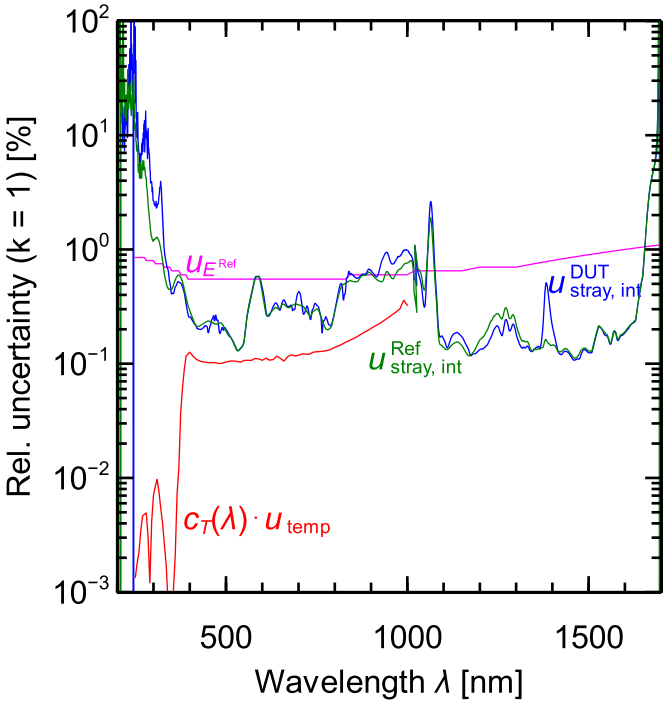

Figure 10. Spectrally dependent input parameters for the uncertainty analysis.

4.2.4. Internal stray light. The uncertainty contribution due to spectral stray light correction is evaluated as outlined in a previous publication [33]. This analysis yields a rectangularly-distributed uncertainty contribution for the spectral stray light correction. The correction introduces correlations over the wavelength intervals 250 nm to 300 nm, 300 nm to 950 nm and 950 nm to 1700 nm. These correlations are taken into account in the uncertainty analysis for $E^{\mathrm{DUT}}_{\lambda}(\lambda)$ by using three random numbers for the corresponding wavelength intervals instead of one for the calculation of $f^{\mathrm{Ref}}_{\mathrm{stray,int}}(\lambda)$ and $f^{\mathrm{DUT}}_{\mathrm{stray,int}}(\lambda)$.

4.2.5. Detector non-linearities. We measure non-linearities with respect to irradiance level using the two lamps-method

as described in appendix D. Non-linearities with respect to integration time are measured using a stable reference lamp. As our spectrometer only shows small non-linearities, which are of the order of measurement uncertainty, we do not apply non-linearity corrections and also neglect the wavelength dependence of these contributions. The observed deviations are considered in the uncertainty analysis by the factors

$$f^{\mathrm{Ref}}_{\mathrm{lin,tint}}(\lambda) = 1 + u_{\mathrm{lin,tint}} \cdot \rho_{\mathrm{lin,tint}} \,, \quad (56)$$

$$f^{\mathrm{DUT}}_{\mathrm{lin,tint}}(\lambda) = 1 + u_{\mathrm{lin,tint}} \cdot \rho_{\mathrm{lin,tint}} \,, \quad (57)$$

$$f^{\mathrm{Ref}}_{\mathrm{lin,irr}}(\lambda) = 1 + u_{\mathrm{lin,irr}} \cdot \rho_{\mathrm{lin,irr}} \,, \quad (58)$$

$$f^{\mathrm{DUT}}_{\mathrm{lin,irr}}(\lambda) = 1 + u_{\mathrm{lin,irr}} \cdot \rho_{\mathrm{lin,irr}} \,, \quad (59)$$

where $u_{\mathrm{lin,tint}}$ and $u_{\mathrm{lin,irr}}$ are relative deviations. The specific values are given in table 1.

4.2.6. Spectral bandwidth. is taken into account using the parameters specified in table 1.

4.2.7. Wavelength accuracy. is taken into account using the parameters specified in table 1.

4.2.8. Spectral irradiance of reference. The uncertainty related to $E^{\mathrm{Ref}}_{\lambda}(\lambda)$ is taken from the calibration certificate issued by PTB.

4.2.9. Distance adjustment. The uncertainty of the distance adjustment is determined by two components, namely the uncertainty of the distance offset correction factor (c_{dist}), which we determine to be 0.78 mm, and the uncertainty of the adjustment (0.1 mm). Both components are rectangularly distributed. Combining the components yields $u_{\mathrm{dist}} = 0.88$ mm as specified in table 1. The distance offset is the dominant component. Hence, u_{dist} is also (approximately) rectangularly distributed.

4.2.10. Variation of lamp operating current. We operate a Quartz-Tungsten-Halogen (QTH) lamp (250 W) with a nominal operating current of $I_{\mathrm{op}} = 9.7$ A at a voltage V_{op} of typically 21.0 V. The uncertainty of the operating current is $u_{\mathrm{cur}} =$ 0.7 mA. This value results from an analysis of the current adjustment accuracy at our facility, which takes the measurement uncertainty of the operating current and the stepwidth of current adjustment by the power supply into account. We obtain an electrical operating power P_{op} of 203.7 W and a filament temperature of $T_{\mathrm{op}} = 3\,462.2$ K. The lamp resistance R_0 measured at room temperature (296.15 K) is 0.15 Ω, the lamp resistance at operating temperature T_{op} is $R(T_{\mathrm{op}}) = V_{\mathrm{op}}/I_{\mathrm{op}} =$ 2.16 Ω. The filament temperature variation due to operation current variations of ±0.7 mA is thus $\delta T = \pm 0.3$ K according to equation (42), resulting in relative deviations of spectral irradiance of 0.14% at 250 nm, 0.07% at 500 nm and 0.02% at 1700 nm. Figure 11 compares the measured spectral irradiance of a typical 250 W QTH reference lamp (symbols) with the blackbody model according to equation (37) (black line), showing that treating the reference lamp as a blackbody radiator is a reasonable approximation for evaluating this uncertainty contribution.

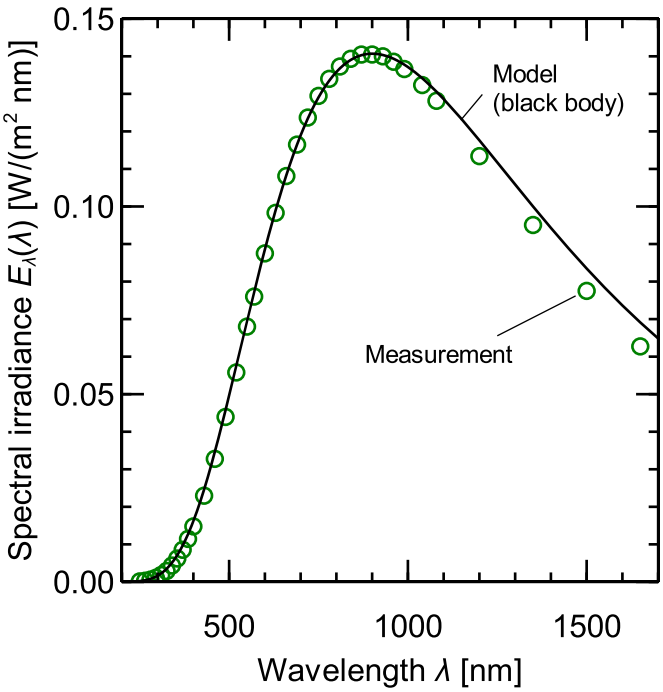

Figure 11. Comparison of the the measured spectral irradiance of a typical 250 W QTH reference lamp (symbols) with the blackbody model according to equation (37) (black line).

4.2.11. Long term reproducibility. This uncertainty contribution is determined from the deviation of the radiometric correction function determined with an identical setup. The specific parameter for the uncertainty calculation is given in table 1.

4.2.12. Detector temperature effects. Since the InGaAs detector of our spectrometer is temperature controlled, we only apply a correction to the signal measured by the silicon detector. We refer the correction to the temperature difference $(T^{\mathrm{DUT}} - T^{\mathrm{Ref}})$ between DUT and reference measurement (typically of the order of 2 K in our laboratory) and thus only apply a correction to the DUT measurement. For the correction, we assume that the origin of the detector's temperature sensitivity is the temperature dependence of the absorption coefficient of silicon α. This assumption has been validated by varying the detector temperature using a hot air fan while measuring the detector signal when being irradiated by a (stable) reference

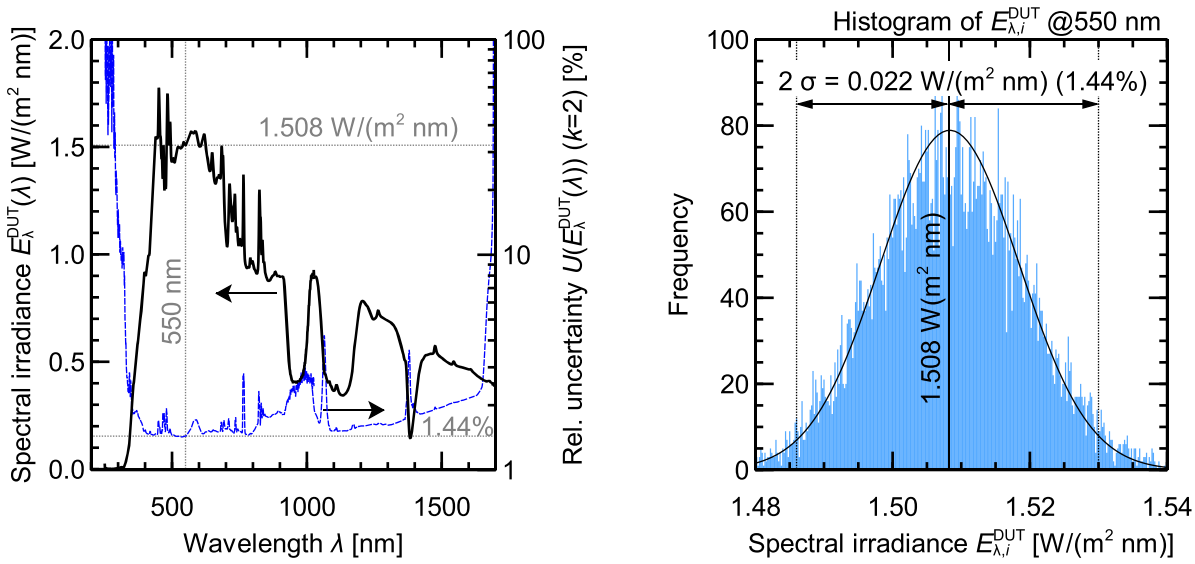

Figure 12. Left: Spectral irradiance of solar simulator (black line) and corresponding relative uncertainty ($k = 2$, dashed blue line). Right: Histogram of $E_{\lambda,i}^{DUT}$ at 550 nm resulting from 10 000 Monte-Carlo iterations. The black curve represents a normal distribution fitted to the data.

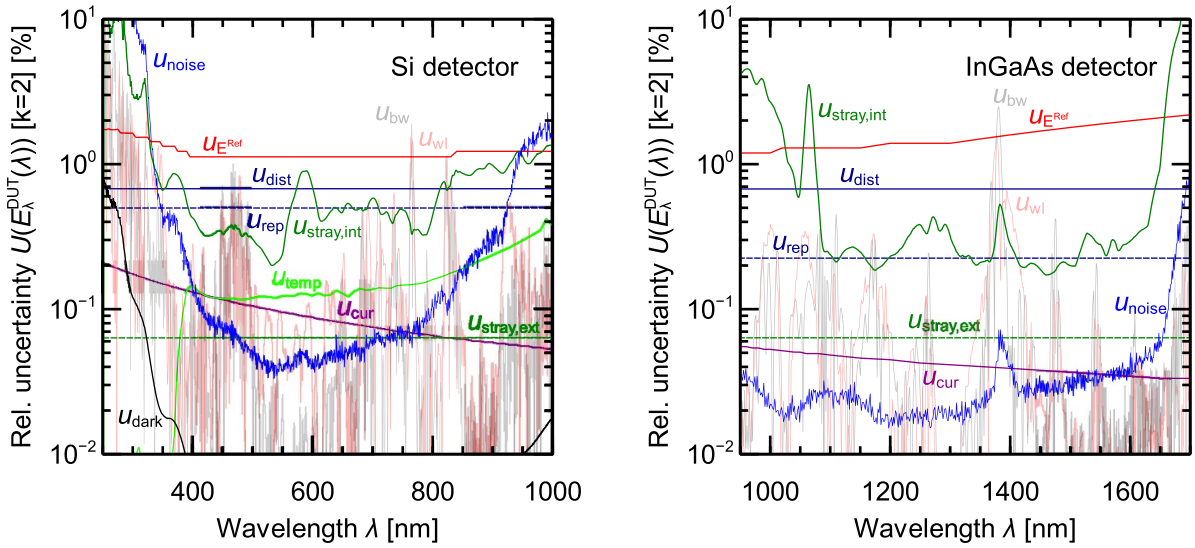

Figure 13. Sensitivity analysis for $U\left(E_\lambda^{DUT}(\lambda)\right)$. Left: Si detector (250 nm–1000 nm). Right: InGaAs detector (950 nm–1700 nm).

lamp. The *relative* temperature coefficient c_T is taken from literature [42] and used for a correction,

$$E_{\lambda,corr}^{DUT}(\lambda) = E_\lambda^{DUT}(\lambda)\left(1 + c_T(\lambda)\cdot\left(T^{DUT} - T^{Ref}\right)\right). \quad (60)$$

We apply the temperature correction to $E_\lambda^{DUT}(\lambda)$ instead of $S_1^{DUT}(\lambda)$ for the sake of simplicity. This is possible because all corrections (including the temperature correction) only have a minor impact on the resulting spectral irradiance. The detector temperature is measured by a Pt1000 temperature sensor, which is attached to the sensor's housing. Therefore, the sensor's chip temperature may slightly deviate from the measured temperature. On the other hand, the temperature measurement is correlated between reference and DUT measurement, so that systematic deviations cancel out. Based on experience, we estimate the overall uncertainty of the temperature difference to be $u_{temp} = 0.3\ ^\circ C$ and include a factor

$$f_{temp}(\lambda) = 1 + c_T(\lambda)\, u_{temp}\cdot\rho_{temp} \quad (61)$$

in the Monte-Carlo analysis. The product $c_T(\lambda)\cdot u_{temp}$ is visualized in figure 10.

4.2.13. Tilt of the measuring head. The alignment on the optical axis is performed by means of a bidirectional alignment laser in such a way that the beam incident on the measuring head is reflected back into itself. The spot size of our laser is 1 mm and the distance between laser and measuring head is about 10 cm during the adjustment. A lateral displacement of the reflected beam of 1 mm on the output window of the laser,

which is clearly visible, thus corresponds to a tilt angle of 0.6° or 0.01 rad, respectively. This value is used as an estimate for u_{tilt}^{X}.

4.2.14. Non-uniformity of the light field and temporal stability of the DUT. Our measurements refer to a specific lateral position in the light field and a specific point of time. Hence, we do not consider these uncertainty contributions.

4.3. Measurement and uncertainty analysis results

Figure 12 (left graph) depicts the measured spectral irradiance $E_{\lambda}^{\mathrm{DUT}}(\lambda)$ of the solar simulator and its relative uncertainty as following from the analysis outlined in section 3. Additionally, the right graph exemplarily shows the distribution of $E_{\lambda,i}^{\mathrm{DUT}}(\lambda)$ at 550 nm (450 bins), from which the values in the left graph are determined using equations (15) and (16). The solid line in the right graph represents a normal distribution fitted to the data. The gaussian shape of the distribution is representative for the whole wavelength range. All calculations are implemented in Python and make use of the standard random number generators included in the NumPy package [43]. The code will be made available on the website of our institute by the time of publication of this paper. Typically, we use $N = 10000$ Monte-Carlo iterations, leading to calculation times of about 3 min on a standard laptop computer.

With respect to a further optimization of the measurement procedure, it is instructive to analyze the impact of the different uncertainty contributions for $E_{\lambda}^{\mathrm{DUT}}(\lambda)$. One option for this, as described in the GUM [17], supplement 1, is setting all but one single uncertainty contribution to zero, running the uncertainty calculation and plotting the result as a function of wavelength. This way, the dominant uncertainty contributions become directly visible. Figure 13 depicts the results of such a calculation for our measurement. On the ordinate, the expanded uncertainty $U\big(E_{\lambda}^{\mathrm{DUT}}(\lambda)\big) = 2\ u\big(E_{\lambda}^{\mathrm{DUT}}(\lambda)\big)$ is plotted, which is obtained if only one uncertainty contribution is considered in the analysis. The plot reveals that dominant uncertainty contributions arise from the calibration of the reference lamp, internal stray light and signal-to-noise ratio in the spectral regions where the sensitivity of the detectors is low. If sharp spectral features are present, spectral bandwidth and wavelength uncertainty also contribute significantly to the overall uncertainty. Note that when considering only one uncertainty component as input, the output quantity $E_{\lambda}^{\mathrm{DUT}}(\lambda)$ is distributed as the corresponding input quantity. Hence, for rectangularly-distributed quantities like $u_{\mathrm{stray,ext}}^{\mathrm{Ref}}(\lambda)$, for instance, the resulting distribution of $E_{\lambda}^{\mathrm{DUT}}(\lambda)$ is also rectangular. In order to properly compare the impact of the different uncertainty components, the standard uncertainty u [17] of $E_{\lambda}^{\mathrm{DUT}}(\lambda)$ must be used, i.e. $u = \sigma$ for normal distributions, $u = a/\sqrt{3}$ for rectangular distributions and $u = a/\sqrt{6}$ for triangular distributions, where σ is the standard deviation and $2a$ is the width of the distribution. In figure 13, this is taken into account. Note that a sensitivity analysis should be regarded as a qualitative tool for improving the measuring procedure.

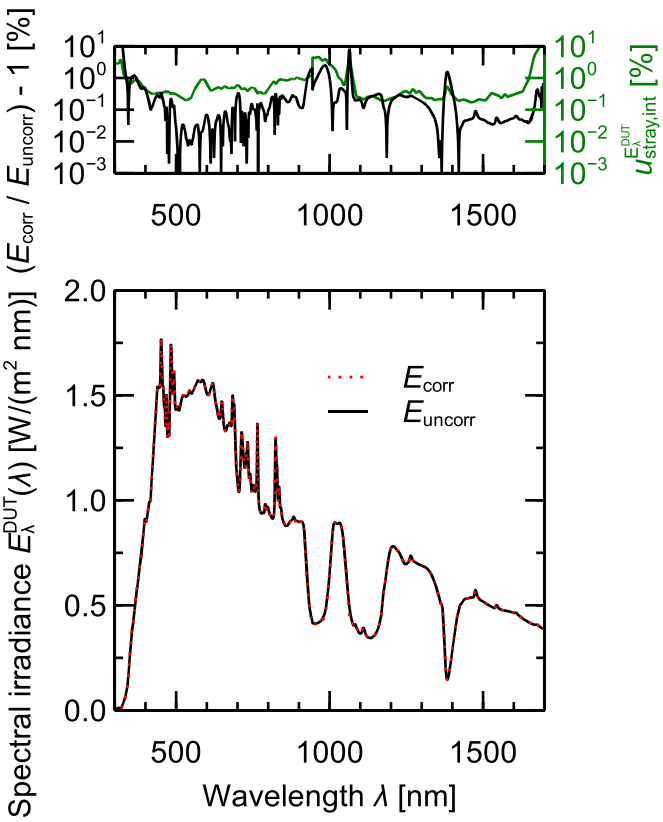

Figure 14. Impact of spectral stray light correction when determining the spectral irradiance of ISFH CalTeC's solar simulator.

Also, note that another option for performing a sensitivity analysis would be setting only one single uncertainty contribution to zero, while all other uncertainty contributions are retained.

Although the implementation of spectral stray light correction into the calculation of $E_{\lambda}^{\mathrm{DUT}}(\lambda)$ is straight forward (matrix multiplication), the experimental effort for the determination of the correction matrix can be enormous and requires an elaborate measurement facility. In practice, this may lead to an imbalance between effort and required accuracy of the measurement. Therefore, it is instructive to look at the overall impact of spectral stray light correction. Figure 14 visualizes the spectral irradiance determined once with ($E_{\mathrm{corr}}(\lambda)$, red dotted line) and once without ($E_{\mathrm{uncorr}}(\lambda)$, black solid line) application of the stray light correction. The top graph shows the absolute amount of relative deviation $\left|\left(E_{\mathrm{corr}}(\lambda)/E_{\mathrm{uncorr}}(\lambda)\right) - 1\right|$ of corrected and uncorrected spectral irradiance and compares it to the relative uncertainty of $E_{\lambda}^{\mathrm{DUT}}(\lambda)$ when only considering the contribution due to the spectral stay light correction (from figure 13). The deviation is mainly below 1% and increases to 10% in the UV region, where the spectral irradiance is low, and around 1050 nm. For most wavelengths, the uncertainty induced by the correction exceeds the impact of the correction itself. Hence, we find that in *this case* the spectral stray light correction has minor impact on the measured spectral irradiance for our solar simulator and spectrometer. However, the uncertainty of the correction must be considered in the uncertainty budget, especially if the correction is neglected. Note

that these results are not necessarily transferable to different solar simulators and/or spectrometers.

5. Conclusion

We presented an in-depth uncertainty analysis for measurements of spectral irradiance caused by direct solar radiation. Fifteen uncertainty sources were discussed in detail and analytical equations for modeling the impact of these uncertainties on the overall uncertainty of the measured spectral irradiance were given. As a specific application example, we described the determination of the spectral irradiance of ISFH CalTeC's solar simulator by means of an array spectrometer and outlined the corresponding measurement uncertainty analysis. The uncertainty is mostly of the order of 2%–3% in the wavelength range from 300 nm to 1700 nm. In the edge-regions, it increases to values of up to about 80% due to noise and stray light. We showed that for this measurement facility, dominant uncertainty contributions arise from the calibration of the reference lamp, internal stray light, signal-to-noise ratio (in regions where the sensitivity of the detectors is low), spectral bandwidth and wavelength uncertainty (in regions where sharp spectral features are present). We also showed that at ISFH CalTeC, the spectral stray light correction does not alter the measured spectral irradiance of the solar simulator significantly. However, this result is not necessarily transferable to different irradiation conditions and/or spectrometers. The uncertainty of the stray light correction must nevertheless be included in the uncertainty budget of the spectral irradiance.

Funding

The project 16ENG02 (PV-Enerate) leading to this publication has received funding from the EMPIR programme co-financed by the Participating States and from the European Union's Horizon 2020 research and innovation programme. Parts of this work were funded by the scholarship program of the german national environmental foundation (Deutsche Bundesstiftung Umwelt).

Acknowledgment

The authors would like to thank H Sträter, S Riechelmann and Peter Sperfeld (PTB) as well as H Müllejans (JRC) for fruitful discussions about the measurement procedure and the uncertainty analysis. The dice and calculator icons in the Monte-Carlo flow chart (figure 3) are provided by *simpleicon.com* and *freesvg.org*.

Appendix A. Monitoring the stability of reference lamps

Reference lamps are usually operated with constant current I_{op}. Many laboratories continuously log the operating current I_{op} and voltage V_{op} measured at the terminals of the lamp in order to monitor the temporal stability of the operating power $P_{\mathrm{op}} = I_{\mathrm{op}} \cdot V_{\mathrm{op}}$ and thus the validity of the spectral irradiance tabulated in the calibration certificate. If the operating power deviates from the value during the calibration, a recalibration may be necessary. Treating the lamp as a blackbody radiator allows to estimate the change of the spectral irradiance caused by a change of the operating power and thereby to define a threshold value for the largest accepted deviation.

In analogy to section 3, we can express the power P as a function of voltage and resistance using Ohm's law and perform a Taylor series expansion around P_{op}:

$$P \approx \frac{V_{\mathrm{op}}^2}{R_{\mathrm{op}}} + \frac{2V_{\mathrm{op}}}{R_{\mathrm{op}}}\,\delta V = P_{\mathrm{op}} + \delta P\,, \tag{A1}$$

where $R_{\mathrm{op}} = V_{\mathrm{op}}/I_{\mathrm{op}}$. From the latter equation,

$$\delta V = \delta P\,\frac{R_{\mathrm{op}}}{2V_{\mathrm{op}}} \tag{A2}$$

follows. Next, we approximate the change of the filament temperature δT in analogy to equations (40) through (42). However, we calculate δT as a function of δV due to the constant current control and obtain

$$\delta T = \frac{\delta V}{I_{\mathrm{op}} R_0 \alpha}\,. \tag{A3}$$

Inserting equation (A2) into equation (A3) yields

$$\delta T = \frac{\delta P}{P_{\mathrm{op}}}\,\frac{R_{\mathrm{op}}}{2R_0\alpha}\,. \tag{A4}$$

With this expression, equation (43) can be used for calculating the change of the spectral irradiance resulting from a change of the electrical power.

For our 250 W QTH reference lamps, we allow a maximum deviation of 0.5 W from the operating power during the calibration before a recalibration is performed. Regarding the example described in section 4, a power deviation of 0.5 W corresponds to a voltage deviation of about 26 mV and a temperature deviation of about 4 K, resulting in a relative deviation of the spectral irradiance of 2.2% at 250 nm, 1.1% at 500 nm and 0.34% at 1700 nm. These deviations are smaller than the measurement uncertainties indicated at these wavelengths, which shows that 0.5 W is a reasonable threshold value for these lamps. Note that voltage deviations are also likely to occur due to thermal expansion inside the terminal blocks of the bulb during the operation of the lamp. This affects the contact resistance but not the filament temperature due to the constant current control. Hence, the threshold value should not be chosen too low. For our lamps, we observe voltage deviations of the order of 15 mV that do not cause measurable deviations of the spectral irradiance and thus are likely due to changes of the contact resistance.

Appendix B. Determination of distance offset

Experimentally, Δd can be determined by varying the distance d between a stable point light source and the measuring head and fitting the relation

$$S(d) = S(d_{\min})\left(\frac{d_{\min}+\Delta d}{d+\Delta d}\right)^2 \tag{B5}$$

to the measured signal $S(d)$ [44, 45], where $d_{\min}$ is the shortest distance chosen in the experiment. For some instruments, a wavelength dependence of Δd may be observed. If the wavelength dependence is not significant (i.e. only leads to small signal deviations compared to the overall measurement uncertainty), a mean value of Δd may be used and deviations of Δd with respect to wavelength may be considered in the uncertainty budget.

Appendix C. Temperature correction

The temperature correction factor $c_{\text{temp}}(\lambda)$ can be determined experimentally by artificially heating the spectrometer while measuring the background-corrected signal $S(\lambda)$ of a stable light source, e.g. a reference lamp. The heating can be performed using a hot air fan or, more accurately, by putting the spectrometer inside a temperature-controlled chamber. From this measurement, the temperature correction coefficient can be deduced:

$$c_{\text{temp}}(\lambda) = 1 + \frac{1}{S(\lambda)}\frac{\partial S(\lambda)}{\partial T}\delta T\,, \tag{C6}$$

where δT should be small compared to the nominal temperature of the spectrometer. This condition is usually fulfilled in air-conditioned laboratories. Special attention to the applicability of the latter equation should be paid under outdoor conditions or if strong radiative heating of the spectrometer by the DUT occurs. The uncertainty $u_{\text{temp}}(\lambda)$ of the temperature correction coefficient arises from the experimental uncertainties during the determination of $c_{\text{temp}}(\lambda)$, in particular: The uncertainty of the temperature deviation δT, the uncertainty of $S(\lambda)$ and the appropriateness of the linear approximation expressed in equation (C6). The standard GUM formalism can be used to combine these uncertainties into the overall uncertainty $u_{\text{temp}}(\lambda)$.

Appendix D. Non-linearity corrections

Determining the spectral irradiance of the DUT according to equation (12) requires a linear behavior of the detector with respect to spectral irradiance and integration time because the spectral irradiance of the reference and DUT can differ by several orders of magnitude, depending on the wavelength. Deviations from a linear characteristic (as exemplary shown in figure D1) would cause a signal deviation, which must be taken into account.

There are several possibilities for the determination of non-linearities related to irradiance variation, e.g. using the inverse square law and varying the distance between light source and detector or using calibrated filters with different attenuation factors. The most accurate determination of non-linearities is facilitated by the superposition method [46] (often also called 'two lamps-method'). This method uses two stable light sources A and B, which illuminate the detector one after the other. Afterwards, both light sources illuminate the detector simultaneously (A+B). The irradiance level on the detector is $E_{\text{A}}(\lambda)$ for the first lamp, $E_{\text{B}}(\lambda)$ for the second lamp and $E_{\text{C}}(\lambda) = E_{\text{A}}(\lambda) + E_{\text{B}}(\lambda)$ for both lamps together. The corresponding detector signals are $S_{\text{A}}(\lambda)$, $S_{\text{B}}(\lambda)$ and $S_{\text{C}}(\lambda)$. Ideally, $S_{\text{C}}(\lambda)$ should be equal to $S_{\text{A}}(\lambda) + S_{\text{B}}(\lambda)$. Deviations from this characteristic lead to the *two lamps-ratio*

$$r_{S_{\text{C}}}(\lambda) = \frac{S_{\text{A}}(\lambda) + S_{\text{B}}(\lambda)}{S_{\text{C}}(\lambda)} \tag{D7}$$

different from unity, which can be interpreted as a *local deviation from linear behaviour* for a given signal level $S_{\text{C}}(\lambda)$.

Figure D1 visualizes the results of the two lamps-method qualitatively for a single wavelength λ_0. A linear detector features a signal $S(\lambda_0)$ that is proportional to the spectral irradiance $E(\lambda_0)$ and thus behaves according to the black line in the upper graph. The green curve represents a quasi-linear

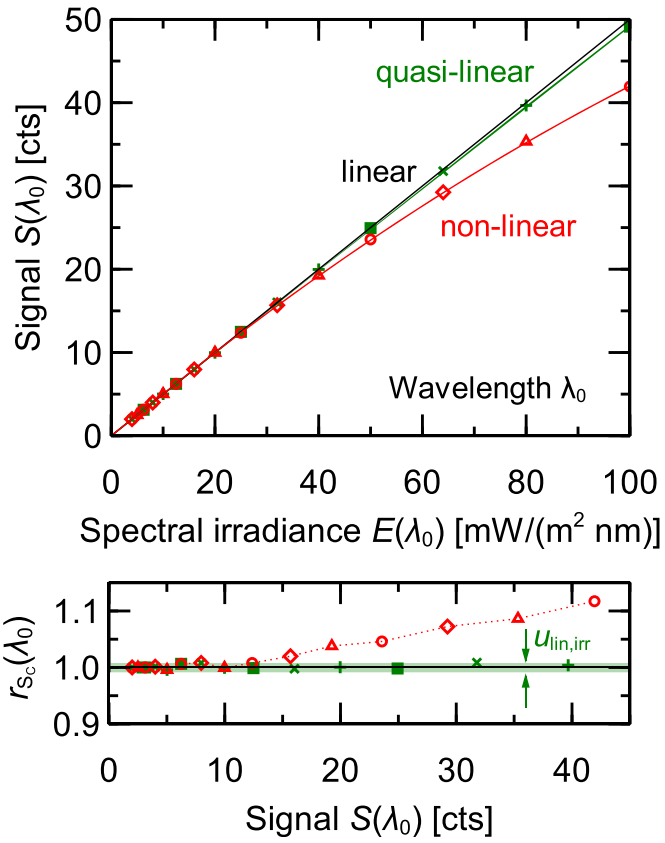

Figure D1. Top: Examplary detector output signal $S(\lambda_0)$ as a function of irradiance level $E(\lambda_0)$ for a linear (black), a quasi-linear (green) and a non-linear detector (red). Bottom: Resulting uncertainty $u_{\text{lin,irr}}(\lambda_0)$ for the quasi-linear detector and non-linearity correction factor $c_{\text{lin,irr}}(\lambda_0)$ for the non-linear detector. The dotted line is a guide to the eye.

detector, which behaves linearly in the low irradiance range and shows small non-linearities at high irradiance. In contrast, the red curve represents a detector showing significant non-linearities. The two lamps-method probes these curves at different signal levels $S_C(\lambda)$, which are represented by the symbols. The different symbols correspond to one measurement series each, where the signal is always doubled. Three measurement series are shown for the quasi-linear and the non-linear case. The lower graph depicts the corresponding ratio $r_{S_C}(\lambda_0)$ as calculated from equation (D7). For the linear device, $r_{S_C}(\lambda_0) \equiv 1$, whereas for the non-linear device, significant deviations from unity are observed. For the quasi-linear device, $r_{S_C}(\lambda_0) \approx 1$ holds.

If no significant non-linearities are observed (green diamonds in lower graph of figure D1), the non-linearity correction factor can be set to unity and the corresponding uncertainty can be defined as the maximum scatter of these data points,

$$u_{\mathrm{lin,irr}}(\lambda) = \max\left(\left|r_{S_C}(\lambda) - 1\right|\right) , \tag{D8}$$

for reasons of simplicity. With this assumtion, the uncertainty is independent of the signal $S(\lambda)$. For the example shown here, the uncertainty is $u_{\mathrm{lin,irr}}(\lambda) = 0.01$. Hence, for the Monte-Carlo uncertainty analysis outlined in section 3, the f-factor would be $f^X_{\mathrm{lin,irr}}(\lambda) = 1 + 0.01\,\rho_{\mathrm{lin,irr}}$. Depending on the spectrometer and the results of the non-linearity measurement, it may be possible to simplify even further by also neglecting the wavelength dependence of the uncertainty. This is a reasonable procedure if $u_{\mathrm{lin,irr}}$ can be estimated conservatively (e.g. as the maximum uncertainty over the whole wavelength range) and the resulting uncertainty contribution is still small compared to other contributions in the uncertainty budget.

If a significant non-linearity is observed (as for the red symbols in the lower graph of figure D1), a non-linearity correction factor $c_{\mathrm{lin,irr}}\big(S(\lambda)\big)$ should be derived and applied. The associated uncertainty is determined by the experimental uncertainties for the determination of $c_{\mathrm{lin,irr}}\big(S(\lambda)\big)$. The determination of the non-linearity correction factor is outlined, e.g. in [46–50]. In order to give a guidance to the reader, we briefly explain a simplified approach for detectors that behave linearly in the low irradiance regime (similar to the example given in figure D1). This usually holds for photodiode- and photodiode array-based spectrometers and thus for a large number of spectrometers that are used throughout the laboratories. We also assume that external stray light is negligible (which can in principal be ensured by an appropriate measurement setup) and that the irradiance levels $E_A(\lambda)$ and $E_B(\lambda)$ on the measuring head are identical (which can in principal be achieved by an appropriate adjustment of the distances between the lamps and the measuring head), leading to $S_A(\lambda) \approx S_B(\lambda)$. The measurement procedure would be as follows:

(a) Lamp A and lamp B are set to the lowest possible irradiance in the linear regime of the detector. The irradiance can be adjusted by changing the distance between lamp and spectrometer and/or by application of neutral density filters. Consequently, the lowest irradiance is determined by the maximum distance possible between the lamp and the detector and/or the highest optical density of the available filters. Since we assume that the detector is linear in the low irradiance regime, the correction factor obtained hereby is

$$c_1\big(S_{C,1}(\lambda)\big) = \frac{S_{A,1}(\lambda) + S_{B,1}(\lambda)}{S_{C,1}(\lambda)} = 1 . \tag{D9}$$

(b) The irradiances of lamp A and B are *doubled* so that

$$S_{A,2}(\lambda) \approx S_{B,2}(\lambda) \approx S_{C,1}(\lambda) \tag{D10}$$

The next correction factor $c_2\big(S_{C,2}(\lambda)\big)$ can then be determined:

$$c_2\big(S_{C,2}(\lambda)\big) = c_1 \cdot \frac{S_{A,2}(\lambda) + S_{B,2}(\lambda)}{S_{C,2}(\lambda)} , \tag{D11}$$

where $c_1 = c_1\big(S_{C,1}(\lambda)\big) = 1$ according to the initial assumption.

(c) Subsequently, the irradiances of lamp A and B are *again doubled*, so that

$$S_{A,3}(\lambda) \approx S_{B,3}(\lambda) \approx S_{C,2}(\lambda) . \tag{D12}$$

Next, the correction factor

$$c_3\big(S_{C,3}(\lambda)\big) = c_2 \cdot \frac{S_{A,3}(\lambda) + S_{B,3}(\lambda)}{S_{C,3}(\lambda)} \tag{D13}$$

is determined. At this point, the correction $c_2 = c_2\big(S_{C,2}(\lambda)\big)$ of the previous measurement, which might deviate from unity, has to be included in order to correct $S_{A,3}(\lambda)$ and $S_{B,3}(\lambda)$ to the linear scale.

(d) This series of measurements is continued until the end of the dynamic range of the detector is reached. This yields the iteratively derived correction factors

$$c_i\big(S_{C,i}(\lambda)\big) = c_{i-1} \cdot \frac{S_{A,i}(\lambda) + S_{B,i}(\lambda)}{S_{C,i}(\lambda)} . \tag{D14}$$

(e) Having finished the series of measurements, it should be verified that the first data point is in the linear regime, i.e.

$$\frac{S_{A,1}(\lambda) + S_{B,1}(\lambda)}{S_{C,1}(\lambda)} \approx 1$$

holds, so that the assumptions on which the procedure is based are fulfilled.

(f) In order to get more data points, the full series can be repeated at different starting points as long as the starting point is located in the linear operating regime of the detector. In figure D1, this is visualized by three different types of symbols, each representing a different series.

(g) The discrete correction factors $c_i\big(S_{C,i}(\lambda)\big)$ can then be interpolated with respect to the signal level in order to obtain the non-linearity correction factor $c_{\mathrm{lin,irr}}\big(S(\lambda)\big)$. The results of this procedure for the non-linear example in figure D1 are depicted in figure D2. The dotted lines represent interpolated values.

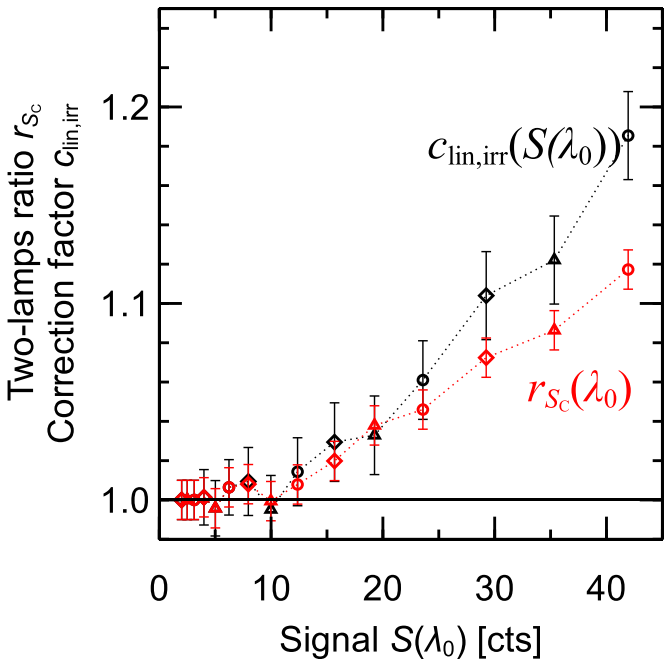

Figure D2. Application of the described measurement procedure to obtain a non-linearity correction function $c_{\mathrm{lin,irr}}(S(\lambda))$ out of the ratios r_{S_C} of the two-lamp data.

For the two lamps-method, irradiance drift, external stray-light, noise and interpolation may contribute to the uncertainty of the non-linearity correction. Since this correction is derived iteratively, the uncertainty increases with increasing irradiance due to uncertainty propagation. This is exemplary shown in figure D2, where the uncertainty of the ratio $r_{S_C}(\lambda_0)$ (represented by the error bars) is constant for each data point. The uncertainty of the non-linearity correction $c_{\mathrm{lin,irr}}(S(\lambda_0))$ then increases with increasing signal. The f-factor for the Monte-Carlo analysis outlined in section 3 would be $f^X_{\mathrm{lin,irr}}(\lambda) = 1 + u_{\mathrm{lin,irr}}(\lambda)/c_{\mathrm{lin,irr}}(\lambda)\,\rho_{\mathrm{lin,irr}}$ according to equation (27). Note that the correction factor $c_{\mathrm{lin,irr}}(\lambda)$ is applied prior to the uncertainty analysis, so that $f^X_{\mathrm{lin,irr}}(\lambda)$ works on the corrected signal and is thus distributed around 1.

Non-linearities related to integration time can be determined in a similar way by variation of the integration time t_{int} at a constant irradiance level (e.g. provided by a stable reference lamp). The analogon to the two-lamps method would be a series of measurements comparing the signal level $S_{\mathrm{C}}(t_{\mathrm{int,C}})$ relative to the signal level $S_{\mathrm{A}}(t_{\mathrm{int,A}}) + S_{\mathrm{B}}(t_{\mathrm{int,B}})$ with the integration time $t_{\mathrm{int,C}} = t_{\mathrm{int,A}} + t_{\mathrm{int,B}}$. This procedure yields the ratios $r(t_{\mathrm{int,C}}, \lambda)$ and consequently the non-linearity correction function $c_{\mathrm{lin,tint}}(t_{\mathrm{int}}, \lambda)$ with respect to integration time. As for the irradiance level, if non-linearities with respect to integration time are observed to be small, no correction is applied and the measured (small) signal deviations are assigned to the uncertainty by

$$u_{\mathrm{lin,tint}}\big(S(\lambda)\big) = \max\left(\Big|r(t_{\mathrm{int,C}}, \lambda) - 1\Big|\right) \tag{D15}$$

for reasons of simplicity. Again, it may be possible to neglect the wavelength dependence, too, as mentioned above.

Appendix E. Spectral bandwidth correction

In this section, a general formula for spectrometer bandwidth correction for generalized bandpass functions is derived following Wooliams *et al* [21]. For comparability, the meaning of the variables in this appendix (especially S) is chosen identically to Wooliams *et al* [21] and shall not be confused with the meaning of variables used throughout the rest of this paper. Moreover, their definition of the spectral bandwidth as the interval $[\lambda - \Delta\lambda, \lambda + \Delta\lambda]$ is adopted for comparability, which differs from the definition $[\lambda - \Delta\lambda/2, \lambda + \Delta\lambda/2]$ used throughout the rest of this paper.

Wooliams *et al* express a measured spectral distribution $M(\lambda)$ at $\lambda = \lambda_0$ by the convolution of the true spectral distribution $S(\lambda)$ with a bandpass function $b(\lambda - \lambda_0)$, wheras the integral of the bandpass function is normalized to one:

$$M(\lambda_0) = \int_{-\infty}^{\infty} S(\lambda)\, b(\lambda - \lambda_0)\, d\lambda\,. \tag{E16}$$

$$1 = \int_{-\infty}^{\infty} b(\lambda - \lambda_0)\, d\lambda\,. \tag{E17}$$

It is assumed that the true spectral distribution can be expanded as a Taylor series at $\lambda = \lambda_0$:

$$S(\lambda) = S(\lambda_0) + (\lambda - \lambda_0)S'(\lambda_0) + \frac{(\lambda - \lambda_0)^2}{2}S''(\lambda_0) + \ldots \tag{E18}$$

Inserting equation (E18) into equation (E16) yields

$$M(\lambda_0) = I_0\, S(\lambda_0) + I_1\, S'(\lambda_0) + \frac{1}{2} I_2\, S''(\lambda_0) + \ldots \tag{E19}$$

with the bandpass moments

$$I_n = \int (\lambda - \lambda_0)^n \cdot b(\lambda - \lambda_0) d\lambda\,. \tag{E20}$$

The expression (E19) can now be rewritten as:

$$\begin{aligned} M(\lambda_0) &= \left(1 + I_1 \frac{d}{d\lambda} + \frac{I_2 d^2}{2 d\lambda^2} + \ldots\right) S(\lambda_0) \\ M(\lambda_0) &= \left(1 + I_1 D + \frac{I_2 D^2}{2} + \ldots\right) S(\lambda_0) \\ M(\lambda_0) &= \Big(1 + C\Big) S(\lambda_0) \end{aligned} \tag{E21}$$

with the operators

$$D = \frac{d}{d\lambda}\,, \tag{E22}$$

$$C = I_1 D + \frac{I_2 D^2}{2} + \ldots\,. \tag{E23}$$

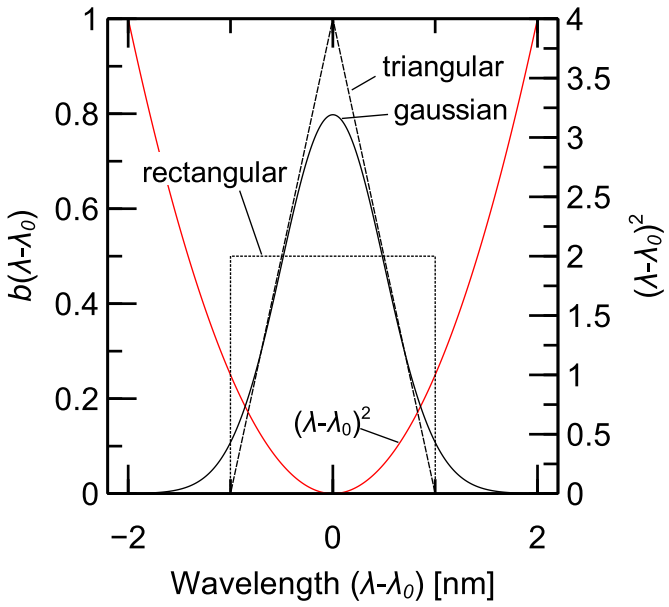

Figure E3. Triangular, rectangular and gaussian shaped bandpass functions $b(\lambda-\lambda_0)$ with identical integral area representing three possible types of spectrometers (here $\lambda_0=0$). The red curve shows the weighting function for the calculations of the moment I_2.

Based on these definitions a new operator

$$F = 1 - C + C^2 - C^3 + \ldots \tag{E24}$$

is defined as the inverse operator of the operator $(1+C)$ which has the property

$$\begin{aligned} F(1+C) &= (1-C+C^2-C^3+\ldots)(1+C) \\ &= 1+C-C-C^2+C^2+C^3-C^3-\ldots \\ &= 1\,. \end{aligned} \tag{E25}$$

Application of F to equation (E21) leads to an expression of the true spectral distribution $S(\lambda_0)$ as a function of the measured spectral distribution $M(\lambda_0)$:

$$S(\lambda_0) = FM(\lambda_0) = (1-C+C^2-C^3+\ldots)M(\lambda_0)\,. \tag{E26}$$

Substiution of equation (E23) into equation (E26) leads to

$$\begin{aligned} S(\lambda_0) &= \left[1-\left(I_1 D+\frac{I_2 D^2}{2}+\ldots\right)\right. \\ &+ \left(I_1 D+\frac{I_2 D^2}{2}+\ldots\right)^2 \\ &- \left.\left(I_1 D+\frac{I_2 D^2}{2}+\ldots\right)^3+\ldots\right]M(\lambda_0)\,. \end{aligned} \tag{E27}$$

This equation can be fully multiplied and sorted in powers of the differential operator D:

$$\begin{aligned} S(\lambda_0) &= \left[1-I_1 D+\left(\frac{-I_2}{2}+I_1^2\right)D^2\right. \\ &+ \left.\left(\frac{-I_3}{6}+I_2 I_3-I_1^3\right)D^3+\ldots\right]M(\lambda_0)\,. \end{aligned} \tag{E28}$$

This formula describes the reconstruction of the true spectral distribution $S(\lambda_0)$ as a function of the measured spectral distribution $M(\lambda_0)$ using the derivatives of the measured spectral distribution and the bandpass moments I_n given in equation (E20). Until now, only the assumption that the true spectral distribution can be evolved in a Taylor series at $\lambda=\lambda_0$ is carried out. In the following, a mathematical simplification is made: Only terms up to the second derivative shall be taken into account. This leads to the final expression

$$S(\lambda_0) = M(\lambda_0) - I_1 M'(\lambda_0) + \left(\frac{-I_2}{2}+I_1^2\right)M''(\lambda_0)\,. \tag{E29}$$

If the bandpass function $b(\lambda-\lambda_0)$ is a symmetrical function with respect to λ_0, the moment

$$I_1 = \int_{-\infty}^{\infty}(\lambda-\lambda_0)\cdot b(\lambda-\lambda_0)d\lambda = 0 \tag{E30}$$

becomes zero and equation (E29) simplifies to

$$\begin{aligned} S(\lambda_0) &= M(\lambda_0) - \frac{I_2}{2}M''(\lambda_0) \\ &= M(\lambda_0)\left(1-\frac{I_2}{2}\frac{M''(\lambda_0)}{M(\lambda_0)}\right)\,. \end{aligned} \tag{E31}$$

The first summand in the latter equation is the signal due to incident light at the nominal wavelength λ_0. The second summand is the additional signal due to light incident at neighbouring wavelengths. The mathematical simplification mentioned above implies that only the two neighboring grid points affect the measured signal at λ_0. This means that equation (E31) is valid only in regions where the spectral bandwidth $\Delta\lambda$ is of the same order of magnitude as the wavelength sampling. If the bandwidth is larger, this formula must be understood as a simplified approximation. For discrete measured signals $M(\lambda)$, the second derivative in equation (E31) can be approximated by [51]

$$M''(\lambda) \approx \frac{M(\lambda-\Delta\lambda)-2M(\lambda)+M(\lambda+\Delta\lambda)}{(\Delta\lambda)^2}\,. \tag{E32}$$

The values $M(\lambda\pm\Delta\lambda)$ required for this calculation can be obtained by linear interpolation of $M(\lambda)$.

In the following, the bandpass moments I_n are calculated for a triangular, a rectangular and a gaussian bandpass function. For comparison of the respective moments $I_{\mathrm{n,tri}}$, $I_{\mathrm{n,rect}}$ and $I_{\mathrm{n,gauss}}$ it is important that these bandpass functions have the same transmission, i.e. integral area. An example for these three different types of bandpass functions with a bandwidths of $\Delta\lambda=1$ nm is shown in figure E3. The dashed curve showes the ideal triangular bandpass function of a monochromator. The plain curve shows a gaussian and the dotted curve a rectangular bandpass function. The red curve shows the weighting function for the calculations of the moment I_2.

E.1. Triangular bandpass

For a triangular bandpass function with an integral value of 1, the function $b_{\mathrm{tri}}(\lambda-\lambda_0)$ is:

$$b_{\mathrm{tri}}(\lambda-\lambda_0)=\begin{cases}\frac{1}{\Delta\lambda}+\left(\frac{\lambda-\lambda_0}{\Delta\lambda^2}\right), & \lambda_0-\Delta\lambda\le\lambda\le\lambda_0\\ \frac{1}{\Delta\lambda}-\left(\frac{\lambda-\lambda_0}{\Delta\lambda^2}\right), & \lambda_0<\lambda\le\lambda_0+\Delta\lambda\\ 0 & \text{elsewhere}\,.\end{cases} \tag{E33}$$

Consequently, the moment I_2 becomes

$$\begin{aligned} I_{2,\mathrm{tri}} &= \int(\lambda-\lambda_0)^2\cdot b((\lambda-\lambda_0))d\lambda\\ &= \int_{\lambda_0-\Delta\lambda}^{\lambda_0}\frac{(\lambda-\lambda_0)^2}{\Delta\lambda}d\lambda+\int_{\lambda_0-\Delta\lambda}^{\lambda_0}\frac{(\lambda-\lambda_0)^3}{\Delta\lambda^2}d\lambda\\ &+ \int_{\lambda_0}^{\lambda_0+\Delta\lambda}\frac{(\lambda-\lambda_0)^2}{\Delta\lambda}d\lambda-\int_{\lambda_0}^{\lambda_0+\Delta\lambda}\frac{(\lambda-\lambda_0)^3}{\Delta\lambda^2}d\lambda\\ &= \frac{1}{3}(\Delta\lambda)^2-\frac{1}{4}(\Delta\lambda)^2+\frac{1}{3}(\Delta\lambda)^2-\frac{1}{4}(\Delta\lambda)^2\\ &= \frac{(\Delta\lambda)^2}{6} \end{aligned} \tag{E34}$$

and the bandpass correction formula (E31) becomes

$$\begin{aligned} S_{\mathrm{tri}}(\lambda_0) &= M(\lambda_0)-\frac{I_2}{2}M''(\lambda_0)\\ &= M(\lambda_0)\left(1-\frac{\mathbf{1}}{\mathbf{12}}(\Delta\lambda)^2\frac{M''(\lambda_0)}{M(\lambda_0)}\right). \end{aligned} \tag{E35}$$

Inserting (E32) into (E35) yields the correction factor $c\_\mathrm{bw}(S,\Delta\lambda)$ defined in (8). Note that (8) applies a different definition of the spectral bandwidth as discussed above. For this reason, $\Delta\lambda$ is replaced by $\Delta\lambda/2$ in (8).

E.2. Rectangular bandpass

For a rectangular bandpass function with an integral value of 1, the function $b(\lambda-\lambda_0)$ is:

$$b_{\mathrm{rect}}(\lambda-\lambda_0)=\begin{cases}\frac{1}{2\Delta\lambda}, & \lambda_0-\Delta\lambda\le\lambda\le\lambda_0+\Delta\lambda\\ 0 & \text{elsewhere}\,.\end{cases} \tag{E36}$$

Please note that here, the full width of the rectangular bandpass function is $2\,\Delta\lambda$ and half of the amplitude compared to the triangular bandpass function in order to have an identical integral area (throughput of the spectrometer) and transmitting wavelength range (see figure E3). Consequently, the moment $I_{2,\mathrm{rect}}$ becomes

$$\begin{aligned} I_{2,\mathrm{rect}} &= \int(\lambda-\lambda_0)^2\cdot b(\lambda-\lambda_0)d\lambda\\ &= \frac{1}{2\Delta\lambda}\int_{\lambda_0-\Delta\lambda}^{\lambda_0+\Delta\lambda}(\lambda-\lambda_0)^2d\lambda\\ &= \frac{1}{6\Delta\lambda}(\lambda-\lambda_0)^3\Big|_{\lambda_0-\Delta\lambda}^{\lambda_0+\Delta\lambda}\\ &= \frac{1}{6\Delta\lambda}\left[\left(\Delta\lambda\right)^3-\left(-\Delta\lambda\right)^3\right]\\ &= \frac{(\Delta\lambda)^2}{3} \end{aligned} \tag{E37}$$

and the bandpass correction formula (E31) becomes

$$\begin{aligned} S_{\mathrm{rect}}(\lambda_0) &= M(\lambda_0)-\frac{I_2}{2}M''(\lambda_0)\\ &= M(\lambda_0)\left(1-\frac{\mathbf{1}}{\mathbf{6}}(\Delta\lambda)^2\frac{M''(\lambda_0)}{M(\lambda_0)}\right). \end{aligned} \tag{E38}$$

E.3. Gaussian bandpass

For a gaussian bandpass function with an integral value of 1, the function $b(\lambda-\lambda_0)$ is

$$b_{\mathrm{gauss}}(\lambda-\lambda_0)=\sqrt{\frac{2}{\pi(\Delta\lambda)^2}}\cdot e^{-\frac{2(\lambda-\lambda_0)^2}{(\Delta\lambda)^2}}. \tag{E39}$$

Please note that here, the variance of the gaussian function is $\sigma=\Delta\lambda/2$ and the integral area (throughput of the spectrometer) for this bandpass function is one in order to satisfy the integral condition (see figure E3). Consequently, the moment $I_{2,\mathrm{gauss}}$ becomes:

$$\begin{aligned} I_{2,\mathrm{gauss}} &= \int(\lambda-\lambda_0)^2\cdot b(\lambda-\lambda_0)d\lambda\\ &= \sqrt{\frac{2}{\pi(\Delta\lambda)^2}}\cdot\int_{-\infty}^{\infty}(\lambda-\lambda_0)^2\cdot e^{-\frac{2(\lambda-\lambda_0)^2}{(\Delta\lambda)^2}}d\lambda\\ &= \ldots\\ &= \sqrt{\frac{2}{\pi(\Delta\lambda)^2}}\cdot\sqrt{\frac{\pi(\Delta\lambda)^6}{4\cdot 8}}\\ &= \sqrt{\frac{(\Delta\lambda)^4}{16}}=\frac{(\Delta\lambda)^2}{4} \end{aligned} \tag{E40}$$

and the bandpass correction formula (E31) becomes

$$\begin{aligned} S_{\mathrm{gauss}}(\lambda_0) &= M(\lambda_0)-\frac{I_2}{2}M''(\lambda_0)\\ &= M(\lambda_0)\left(1-\frac{\mathbf{1}}{\mathbf{8}}(\Delta\lambda)^2\frac{M''(\lambda_0)}{M(\lambda_0)}\right). \end{aligned} \tag{E41}$$

In summary, the corresponding factors in the bandwidth correction formula increase from 1/12 for a triangular bandpass function via 1/8 for a gaussian bandpass function to 1/6 for a rectangular bandpass function. This reflects the increasing impact of the additional signal contribution from neighbouring wavelengths.

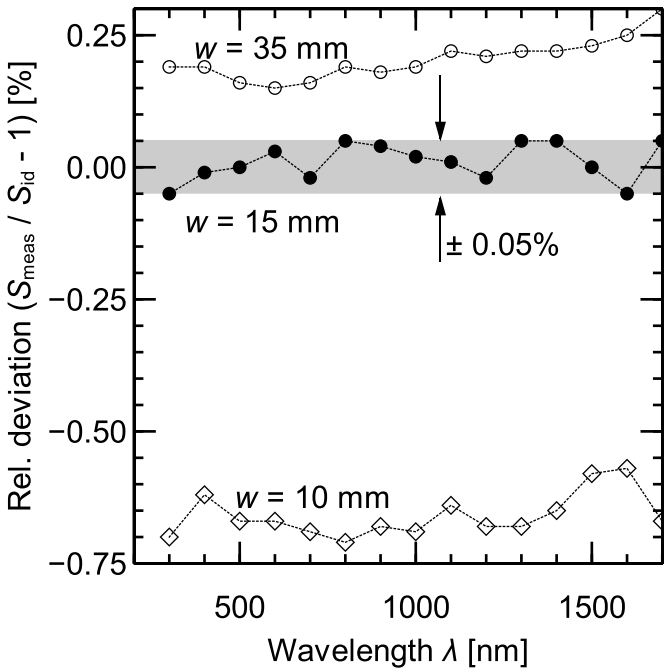

Figure F4. Relative deviation of the measured signal (including external stray light correction) from the ideal signal as calculated with the ray tracing simulation.

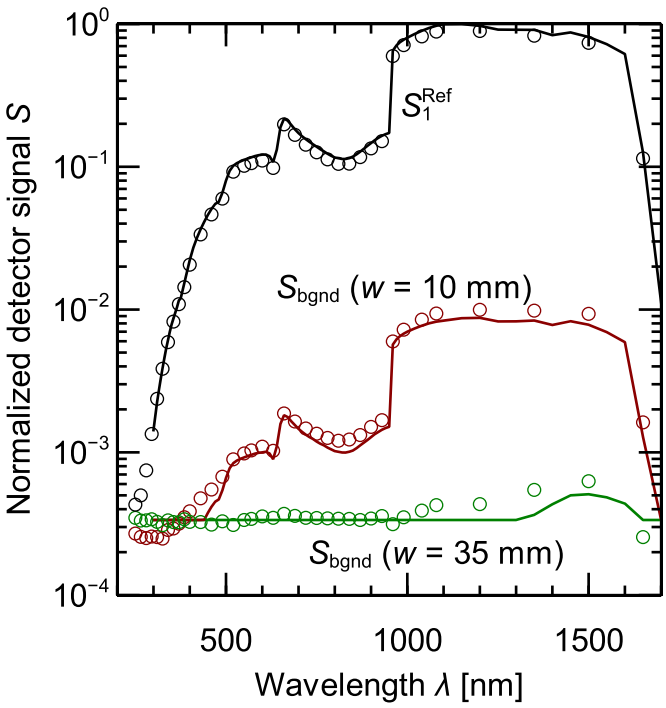

Figure F5. Validation of the external stray light simulation. Open symbols depict measured values, solid lines depict the corresponding calculated values.

Appendix F. External stray light simulation

We model the geometry of the measuring facility using measured reflectance data for the objects and take the measured lateral and angular sensitivity of the measuring head into account. A total of 10^9 rays are simulated for each wavelength (step-width 100 nm), leading to computation times of the order of several hours when using parallelization on 12 processor cores. Figure F4 shows the resulting deviation of the measured signal from between the ideal signal for the beam block used (width $w = 15$ mm, black circles). For comparison, the simulation results for two different beam blocks (10 mm and 35 mm, open symbols) are included. The deviation is below $\pm 0.05\%$ and does not show a systematic trend. The other widths of the beam block lead to over- or undercorrection of external stray light. The noisy appearance of the curves is a consequence of the small fraction of light rays ($< 0.003\%$) hitting the measuring head when the beam block is mounted. The noise reflects the random nature of the Monte-Carlo ray tracing approach [52] and could be reduced by using more light rays for the simulation. However, we refrain from that, since the maximum deviation observed is not a limiting uncertainty contribution, and use 10^9 light rays as a sufficient trade-off between accuracy of the simulation and computational effort. From figure F4, we deduce a *relative* uncertainty of $S_4^{\mathrm{Ref}}(\lambda)$ of

$$u_{\mathrm{stray,ext}}^{\mathrm{Ref}} = 0.000\,5\,, \tag{F42}$$

where we neglect the wavelength dependence for reasons of simplicity.

The simulation is validated by measuring the detector signal with and without beam block in the beam path (illuminated signal $S_1^{\mathrm{Ref}}(\lambda)$ and background signal $S_{\mathrm{bgnd}}(\lambda)$, respectively) for the widest (35 mm) and smallest (10 mm) beam block. From the simulation, a detection probability $f_{\mathrm{det}}(\lambda)$ is calculated for light rays emitted by the light source when the beam block is placed in the beam path. The background signal is then calculated from the illuminated signal by multiplication with $f_{\mathrm{det}}(\lambda)$ from the simulation and compared to the measured background signal. The result of this validation is depicted in figure F5 (open circles: measured values, solid lines: corresponding calculated values $S_{\mathrm{bgnd}}(\lambda) = S_1^{\mathrm{Ref}}(\lambda) \cdot f_{\mathrm{det}}(\lambda)$), demonstrating that the calculated detection probability is of the correct order of magnitude and that the simulation thus properly models the optical properties of the measurement setup.

ORCID iDs

Carsten Schinke https://orcid.org/0000-0002-0740-8733
David Hinken https://orcid.org/0000-0003-4340-0859
Karsten Bothe https://orcid.org/0000-0001-9369-2429

References

[1] Galleano R *et al* 2015 Second international spectroradiometer intercomparison: results and impact on pv device calibration *Prog. Photovolt. Res. Appl.* **23** 929–38
[2] Galleano R *et al* 2016 Results of the fifth international spectroradiometer comparison for improved solar spectral irradiance measurements and related impact on reference solar cell calibration *IEEE J. Photovolt.* **6** 1587–97

[3] Galleano R *et al* 2019 Spectroradiometer comparison under outdoor direct normal irradiance and indoor highpower am0-like conditions *36th European Photovoltaic Solar Conf. and Exhibition* pp 1460–5

[4] Thuillier G, Hersé M, Labs D, Foujols T, Peetermans W, Gillotay D, Simon P C and Mandel H 2003 The solar spectral irradiance from 200 to 2400 nm as measured by the solspec spectrometer from the atlas and eureca missions *Sol. Phys.* **214** 1–22

[5] Myers D R, Reda I, Wilcox S and Andreas A 2004 Optical radiation measurements for photovoltaic applications: instrumentation uncertainty and performance *Proc. SPIE* **5520**

[6] Park S, Lee D-H, Kim Y-W and Park S-N 2007 Uncertainty evaluation for the spectroradiometric measurement of the averaged light-emitting diode intensity *Appl. Opt.* **46** 2851–58

[7] Hohl-Ebinger J and Warta W 2011 Uncertainty of the spectral mismatch correction factor in stc measurements on photovoltaic devices *Prog. Photovolt. Res. Appl.* **19** 573–9

[8] Cordero R R, Seckmeyer G, Riechelmann S, Damiani A and Labbe F 2012 Monte carlo-based uncertainty analysis of UV array spectroradiometers *Metrologia* **49** 745–55

[9] Dubard J and Etienne R 2013 A guide for the evaluation of the solar spectrum measurement uncertainty using array spectroradiometers *Technical report* EURAMET

[10] Dubard J, Etienne R and Valin T 2014 Uncertainty evaluation of spectrally resolved source output measurement using array spectroradiometer *Proc. CIE Symp. on Measurement Uncertainties in Photometry and Radiometry for Industry*

[11] Bohn B and Lohse I 2017 Calibration and evaluation of ccd spectroradiometers for ground-based and airborne measurements of spectral actinic flux densities *Atmos. Meas. Tech.* **10** 3151–74

[12] Galleano R, Kröger I, Plag F, Winter S and Müllejans H 2018 Traceable spectral irradiance measurements in photovoltaics: Results of the ptb and jrc spectroradiometer comparison using different light sources *Measurement* **124** 549–59

[13] Tatsiankou V, Hinzer K, Schriemer H, Kazadzis S, Kouremeti N, Gröbner J and Beal R 2018 Extensive validation of solar spectral irradiance meters at the world radiation center *Sol. Energy* **166** 80–9

[14] Schmähling F, Wübbeler G, Krüger U, Ruggaber B, Schmidt F, Taubert R D, Sperling A and Elster C 2018 Uncertainty evaluation and propagation for spectral measurements *Color Research & Application* **43** 6–16

[15] Gröbner J and Kouremeti N 2019 The precision solar spectroradiometer (psr) for direct solar irradiance measurements *Sol. Energy* **185** 199–210

[16] Kärhä P, Vaskuri A, Mäntynen H, Mikkonen N and Ikonen E 2017 Method for estimating effects of unknown correlations in spectral irradiance data on uncertainties of spectrally integrated colorimetric quantities *Metrologia* **54** 4

[17] Document produced by Working Group 1 of the Joint Committee for Guides in Metrology (JCGM/WG 1) 2008 *Guide to the Expression of Uncertainty in Measurement* (Paris: BIPM)

[18] Zong Y, Brown S W, Carol Johnson B, Lykke K R and Ohno Y 2006 Simple spectral stray light correction method for array spectroradiometers *Appl. Opt.* **45** 1111–19

[19] Stearns E I and Stearns R E 1988 An example of a method for correcting radiance data for bandpass error *Color Res. Appl.* **13** 257–9

[20] Gardner J L 2006 Bandwidth correction for LED chromaticity *Color Res. Appl.* **31** 374–80

[21] Wooliams E R, Baribeau R, Bialek A and Cox M G 2011 Spectrometer bandwidth correction for generalized bandpass functions *Metrologia* **48** 164–72

[22] Nevas S, Wübbeler G, Sperling A, Elster C and Teuber A 2012 Simultaneous correction of bandpass and stray-light effects in array spectroradiometer data *Metrologia* **49** 43–7

[23] International Electrotechnical Commission 2009 *International Standard IEC 60904-7:2009* Geneva, Switzerland

[24] Seckmeyer G and Bernhard G 1993 Cosine error correction of spectral UV-irradiances *Proc. SPIE* **2049**

[25] Feister U, Grewe R and Gericke K 1997 A method for correction of cosine errors in measurements of spectral uv irradiance *Sol. Energy* **60** 313–32

[26] Pulli T, Kärhä P and Ikonen E 2013 A method for optimizing the cosine response of solar uv diffusers *J. Geophys. Res.: Atmos.* **118** 7897–904

[27] Devroye L 1986 *Non-Uniform Random Variate Generation* (Berlin: Springer)

[28] Bratley P, Fox B L and Schrage L E 1987 *A Guide to Simulation* (Berlin: Springer)

[29] Sperling A, Larionov O, Grusemann U and Winter S 2005 Stray-light correction of array spectroradiometers using tunable pulsed and cw lasers *Proc. of the 9th Int. Conf. on New Developments and Applications in Optical Radiometry* Davos, Switzerland

[30] Kreuter A and Blumthaler M 2009 Stray light correction for solar measurements using array spectrometers *Rev. Sci. Instr.* **80** 096108

[31] Salim S G R, Fox N P, Hartree W S, Woolliams E R, Sun T and Grattan K T V 2011 Stray light correction for diode-array-based spectrometers using a monochromator *Appl. Opt.* **50** 5130–38

[32] Nevas S, Gröbner J, Egli L and Blumthaler M 2014 Stray light correction of array spectroradiometers for solar uv measurements *Appl. Opt.* **53** 4313–9

[33] Schinke C, Franke M, Bothe K and Nevas S 2019 Implementation and uncertainty evaluation of spectral stray light correction by zong's method *Appl. Opt.* **58** 9998–10009

[34] Bousquet P 1971 *Spectroscopy and its Instrumentation* (Adam Hilger)

[35] Sansonetti C J, Salit M L and Reader J 1996 Wavelengths of spectral lines in mercury pencil lamps *Appl. Opt.* **35** 74–7

[36] Burgess C and Hammond J 2007 Wavelength standards for the near-infrared spectral region *Spectroscopy* **22** 40–8

[37] Planck M 1901 Ueber das gesetz der energieverteilung im normalspectrum *Ann. Phys. Lpz.* **4** 553–63

[38] International Electrotechnical Commission 2019 *International Standard IEC 60904-3:2019 (edn 4.0)* Geneva, Switzerland

[39] International Electrotechnical Commission 2007 *International Standard IEC 60904-9:2007 (edn 2.0)* Geneva, Switzerland

[40] Nevas S, Lindemann M, Sperling A, Teuber A and Maass R 2009 Colorimetry of leds with array spectroradiometers *Mapan* **24** 153

[41] Holst H, Winter M, Vogt M, Bothe K, Köntges M, Brendel R and Altermatt P P 2013 Application of a new ray tracing framework to the analysis of extended regions in Si solar cell modules *Energy Procedia* **38** 86–93

[42] Green M A 2008 Self-consistent optical parameters of intrinsic silicon at 300 K including temperature coefficients *Sol. Energ. Mat. Sol.* C. **92** 1305–10

[43] The SciPy community Numpy manual https://numpy.org/doc/stable/reference/random/index.html

[44] Hovila J, Mustonen M, Kärhä P and Ikonen E 2005 Determination of the diffuser reference plane for accurate

illuminance responsivity calibrations *Appl. Opt.* **44** 5894–8
[45] Gröbner J and Blumthaler M 2007 Experimental determination of the reference plane of shaped diffusers by solar ultraviolet measurements *Opt. Lett.* **32** 80–2
[46] Coslovi L and Righini F 1980 Fast determination of the nonlinearity of photodetectors *Appl. Opt.* **19** 3200–3
[47] Sanders C L 1962 A photocell linearity tester *Appl. Opt.* **1** 207–11
[48] Boivin L P 1993 Automated absolute and relative spectral linearity measurements on photovoltaic detectors *Metrologia* **30** 355
[49] International Electrotechnical Commission 2019 *International Standard IEC 60904-10:2019 (edn 3.0)* Geneva, Switzerland
[50] Müllejans H and Salis E 2019 Linearity of photovoltaic devices: quantitative assessment with n-lamp method *Meas. Sci. Technol.* **30** 065008
[51] Bronstein I N and Semendjaev K A 2001 *Taschenbuch der Mathematik* (Verlag Harri Deutsch) 5th edn p 931
[52] Schinke C, Vogt M R and Bothe K 2018 Optical modeling of photovoltaic modules with ray tracing simulations Freunek M ed. *Photovoltaics Modeling Handbook* (Whiley/Scrivener)